SYNTHESIS AND OPTICAL CHARACTERIZATION OF CHITOSAN CAPPED GOLD NANOPARTICLES VIA CHEMICAL REDUCTION TECHNIQUE

NORFAZILA MOHD SULTAN

UNIVERSITY OF MALAYA

DECLARATION

I hereby declare that the work in this thesis is my own except the quotations and summaries which have been duly acknowledged.

11 August 2012 NORFAZILA BINTI MOHD SULTAN

KGA 080079

ACKNOWLEDGEMENT

I would like to express my gratitude to Dr. Mohd Rafie Johan, my respectable supervisor for his persistant guidance, assistance and support during execution of my master of degree of work. I am really indebted to him for his encouragement, availability for discussion even during holidays. His honesty,work ethics and sincerity of conducts have become excellent examples for me to follow.

I wish to thank my fellow friends, Nurulhawa Ali, Rosnaini Saidan, Siti Hajar Mohd Noor, Aemi Nadia Ahmad Sauffi, Nurin Zulkifli, Sharidah Azuar abd Azis, Nor Wahida Ahmad for their helpfulness for sharing knowledge and availability to answer my questions. My heartiest thanks are extended to the academic and administrative staffs at the Department of Mechanical Engineering for their continuing support.

Last but not least, my heartfelt thanks goes to my parents, brother and husband for their never ending support, sturdy patience, tones of prayers which gave me strength and motivation to finishes up my studies.

Lastly, may this invention to science bring us closer to Creator himself and understand the

universe.

ABSTRACT

The simple route of synthesizing gold nanoparticles via chemical reduction technique was implemented. The main focus of this study is to achieve enhanced properties of gold nanoparticles by regulating the process parameters of the synthesis. The correlation of the process parameters and resultant size of gold nanoparticles has been deliberated. The gold nanoparticles were reduced with monosodium glutamate (MSG) and further capped with chitosan to prevent agglomeration between particles. The samples were characterized with several characterization techniques. The TEM micrograph showed dispersed particles with narrow size distribution of capped gold nanoparticles with the most probable particles size distributed in the range of 16 to 18 nm. The most stable gold nanoparticles occurred after reduced with 100 mM of MSG and capped with 1g of chitosan where the SPR peaks were blue shifted as the concentration of reducing agent increases and decreasing pattern of FWHM was recorded. Gold nanoparticles capped with chitosan remain small in size after aged for 1 month compared to uncapped gold nanoparticles. Gold nanoparticles exhibit sharper absorbance peak at longer relaxation time. The Gibbs free energy (GFE) of

chitosan-capped gold nanoparticles reduced with 50 mM of MSG calculated as 12.22 KJ/mol and the equilibrium constant, K_{eq} was computed to be 0.0219 mol L^{-1}. The ability of chitosan capped gold nanoparticles to uptake analytes was studied by employing amorphous carbon nanotubes (α- CNT), copper oxide (Cu_2O) and zinc sulphate ($Zn\ SO_4$) as the target materials. The absorption spectra showed dramatic peak intensity increased and red shifted SPR peak once the analytes were added to the chitosan capped gold nanoparticles.

ABSTRAK

Kaedah termudah untuk sintesis zarah nano emas melalui keadah penurunan kimia telah diaplikasikan. Zarah nano emas diturunkan dengan menggunakan monosodium glutamate (MSG) dan kemudiannya dilindungi dengan chitosan. Sampel seterusnya telah dikaji dengan beberapa instrumentasi. Mikrograf TEM menunjukkan zarah nano emas dilindungi chitosan menjauhi antara satu sama lain dan mempunyai pengagihan saiz yang kecil dengan purata saiz di antara 16 ke 18 nm. Kepekatan agen penurunan dan berat chitosan dipelbagaikan untuk membolehkan analisis yang lebih mendalam. Puncak penyerapan telah beralih ke biru graf apabila kepekatan agen penurunan ditambah menghampiri 300mM menandakan pengecilan purata saiz zarah nano emas. Zarah nano emas diturunkan dengan MSG berkepekatan 100 mM dan seterusnya dilindungi dengan chitosan seberat 1 g adalah paling stabil di mana puncak SPR telah membuat peralihan biru apabila kepekatan agen penurunan bertambah dan FWHM dilihat semakin menurun. Zarah nano emas yang dilindungi chitosan dikaji telah mengekalkan saiznya selepas 1 bulan tanpa pembesaran yang ketara berbanding zarah yang tidak dilindungi chitosan. Pada masa rehat yang lebih panjang, zarah nano emas mempamerkan puncak penyerapan yang lebih tirus. Nilai tenaga bebas Gibbs bagi zarah nano emas yang dilindungi chitosan ialah 12.22 $kJmol^{-1}$ dan pekali kestabilan, K_{eq} ialah 0.0219 mol L^{-1}. Kebolehupayaan zarah nano emas dilindungi dengan chitosan untuk mengesan analit telah dikaji dengan tiub karbon nano amorfus (α-CNT), copper oxide (Cu_2O) and zink sulfat (Zn_2 SO_4) sebagai bahan sasaran. Puncak penyerapan untuk semua bahan diperhatikan menambah kepekatan dan beralih ke merah apabila jumlah bahan sasaran ditambah.

TABLE OF CONTENTS

LIST OF PAPERS SUBMITTED FROM THIS WORK

1. **N.M. Sultan** and M.R. Johan, "Chitosan Capped Gold Nanoparticles: An Optical Studies", Int. J. Mol. Sci. (**IJMS-22434: submitted**)

2. **N.M. Sultan** and M.R. Johan, "Effect of amorphous-carbon nanotube (α-CNTs)s, oxides and sulphate to chitosan capped gold nanoparticles", Journal of Luminescence (**under preparation**)

Paper presented from this work:

1. "The Effect Of Chitosan On The Phsyical And Optical Of Gold Nanoparticles", Presented at Symposium B Nanomaterials for Bioimaging and Biosensing, International Conference on Materials for Advanced Technologies (ICMAT 2009).

2. **"**Preparation And Stabilization Of Mono Disperse Colloidal Gold Nanoparticles By Reduction With MSG And Stabilized With Chitosan" Presented at 4thInternational Conference on Advanced Computational Engineering and Experimenting (ACE-X 2010)

LIST OF FIGURES

LIST OF TABLE

LIST OF SYMBOLS

A	Absorbance (a.u)
G	Gibbs free energy (KJ mol^{-1})
I	Intensity of transmitted radiation (a.u)
I_o	Incident radiation (a.u)
K_{eq}	Equilibrium constant
ℓ	Sample cell length
n	Order of reflection
R	Gas constant
T	Ambient temperature
x	Concentration of gold nanoparticles complex

Greek letters

ε_c	Extinction coefficient
λ	Wavelength of x-ray radiation source
π	Pi

LIST OF ABBREVIATIONS

$AuCl_3$	Gold (III) Chloride
AuNp	Gold Nanoparticles
α-CNTs	Amorphous Carbon Nanotubes
Cu_2O	Cooper (II) Oxide
$Zn\ S0_4$	Zinc Sulphate
MSG	Monosodium Glutamate
FWHM	Full-width at half maximum
IR	Infrared
TEM	Transmisson Electron Microscope
UV-Vis	UV-Visible
TAA	Thioacdetamide
CS_2	Carbon Disulfide
NH_2	Amino
COOH	Carboxylic acid
SH	Mercapto
CN	Cyano
CTAB	Cetyltrimethylammonium Bromide
Ppm	Parts per millions
SPR	Surface Plasmon Resonance

Chapter One

INTRODUCTION

CHAPTER ONE

Introduction

1.0 Background of study

Gold nanoparticles (Au NPs) have glowing prospects in many applications due to their distinctive optical properties (Handley, 1989) and expediency of surface bioconjugation with molecular probes (Bendayan, 1981). The promising applications comprise of biosensing (Wang et al., 2007), immunoassays (Saleh et al., 2011), clinical chemistry (Pedro et al., 2006), detection and control of microorganisms (Wang et al., 2008), targeted delivery of drugs or substances (Park et al., 2009), optical imaging and monitoring of biological call and tissues (Zhang et al., 2009), optical coherence tomography (Leon et al., 2011) and two photon luminescence photoacoustics (Durr et al., 2007). Au NPs display intense colours when induced by incident light field. These were contributed by collective electron oscillation that gives intensification to the surface plasmon resonance (SPR) (Hoffman, 2010).

Numerous routes have been proposed for the formation of nano-sized gold. For instance, physical methods such as photochemistry at UV and near IR resonance (Scaiano et al., 2009), sonochemistry (Yong et al., 2007), radiolysis (Dawson & Prashant,2000) and thermolysis (Nakamoto et al., 2002) have been implemented in manufacturing of Au NPs. Furthermore, the use of microemulsions (Rajput et al., 2009), reversed micelles (Herrera et al., 2005), membranes (Markowitz,et al., 1999), seeding growth (Nikhoobakht & El-Sayed, 2003) and polyelectrolytes (Svergun et al., 1998) have been utilized to reduce the size. Among them, the simplest and economical route was chemical reduction which have been utilised in this work. The chemical reduction method for gold nanoparticles basically initiated by reduction of gold precursor to zerovalent Au^0 from Au^{3+}.

The invention of zerovalent gold colloids was pioneered by Turkevich (1951) and latter refined by Frens (1972), in which the ratio of gold precursors to citrate was varied. Brust-Schiffrin (1994) commenced the synthesis of Au NPs in organic solvents which involves a phase transfer agent such as toluene (Daniel & Astruc 2004). The above conventional methods had many shortcomings which contributed to explorations of other reducing agents and alternative routes. The synthesis through Turkevich approaches take a longer time (1 hour) for gold salt reduction. While, the use of organic solvents in Brust-Schiffrin method leave them inapt for biological applications (Dutta et al., 2005). Sugunan and Dutta (1999) have reported the synthesis of nanosized gold in which the gold salt reduction time are less than 1 hour in a single pot process and the resulting particles fits for biological applications.

Various chemicals had been exploited as reducing agent to produce zerovalent gold colloids

including amino acid derivatives. Among the amino acid derivatives reported from subsequent finding, lycine and valine were tried without success. This convinced that only acidic amino acid derivatives such as aspartic acid (Mandal et al., 2002) and monosodium glutamate (Sugunan & Dutta, 1999) are competent in reducing gold salt. Dutta et al (2005) attempted reduced Au NPs by monosodium glutamate by emphasizing on smaller molar ratios of monosodium glutamate (Sugunan & Dutta, 1999). In these research works, the reduction of Au NPs with higher molar ratio of monosodium glutamate had been carried out in order to study the behavior and efficiency of Au NPs and reductant.

Au NPs have compelling tendency to flocculate and immerse due to their Van der Walls interactions. Agglomeration can be hindered by introducing a repulsive force between the particles (Sugunan & Dutta 1999). Chitosan was used as a stabilizer like Warad et al. (2004) reported ZnS nanoparticles doped with manganese were capped with chitosan. The nanoparticles were stabilized by steric hindrance which is contributed by chitosan. The amino group presence in its polycationic structure activates steric hindrance, thus ensures strong stability over long durations (Warad et al., 2004). For most biological applications, many attractive functional group such as biotin (Nath & Chilkoti, 2004), aptamers (Pavlov et al., 2004; Huang et al., 2005), concanavalin (con-A) (Hone et al., 2003), bovine serum albumin (Fujiwara et al., 2006; Frederix et al., 2003), hyperbranched polymer (Luo & Do, 2004) and optical fibres (Mayer et al., 2008; Cheng & Chau, 2003) have been utilized (Kim et al., 2006). However, proteins have a disadvantage as it is expensive although it was widely exploited and offer excellent characteristics. Remarkably, chitosan possesses similar ability as proteins to reduce gold salt and manipulations of its properties have not been fully utilized. Its ready accessible for cross linking through its boundless amino group and its

cationic features which allows ionic cross linking to take place with multivalent. The most promising features of chitosan was its solubility in aqueous acidic solutions replacing the utilization of hazardous organic solvents (Mi et al., 1999), (Guibal, 2004). The properties of chitosan agrees with the aims of the research to manufacture a readily biocompatibles and non toxic chitosan capped Au NPs.

Dutta et al. (2005) had employed chitosan as a sensor for heavy metal ions yet its proficiency thermodynamically not known. The performance of chitosan adsorption on the surface of Au NPs has not been studied quantitatively using extended Benesi-Hildebrand method. This method has been reported with thioacdetamide (TAA) conjugated Au NPs (Kuno, 2007).

In this research work, Au NPs was prepared in one-pot synthesis by utilization of monosodium glutamate (MSG) as reductant and chitosan as capping agent. The effectiveness of these two components towards Au NPs was briefly studied. The correlation of the parameter was experimented and the size dependence was thoroughly monitored. The efficiency of resultant chitosan capped Au NPs towards chemical analytes was attested.

1.1 Important Research Problems

The main problem in synthesizing Au NPs is to control the stability of particles from agglomeration. The problem gives significant impact to the properties of Au NPs. It also gives restriction to the Au NPs from further functionalization process and other applications. Hence, it is essential to discover a better combination of reducing agent, chemical reagent, synthesis procedure and capping agent in order to achieve sterically hindered particles. Previous works have shown the electrostabilization mechanism which controls the stability of particles through van de Waals interaction (Hiemenz,1977). Although this mechanism imparts stability, particles which are sterically hindered have superior performance in preserving anti-agglomeration.

Agglomeration has many drawbacks including wider distribution of size. This contributes to the defile of the colloidal particles homogenity. Thus, the effectiveness of Au NPs and chitosan capped Au NPs are neglected. The homogeneity could be achieved by controlling the key parameters such as type of the solvents, reducing agent concentration and temperature. They are essential to meet the fast paced industrial demands. In these research works, key parameters has been highlighted as the heart of the work to ensure the effectiveness of Au NPs and chitosan Au NPs preserved.

Monosodium glutamate and chitosan are classified as biological compatible compounds. These compounds are preferred for biological applications since they are nontoxic. Several works have shown the utilization of toxic reducing agent, capping agent and reaction medium throughout the synthesis process. These restrict the implementation of Au NPs and

chitosan capped Au NPs for medicinal and biological applications giving windows of opportunity to find much less toxic reducing and capping agents.

Au NPs and chitosan capped Au NPs have been utilized in wide range of applications. Nevertheless, many efforts have been carried out to accomplish superior performance of Au NPs and chitosan capped Au NPs. Subsequently, this research would highlight the capability of resultant chitosan capped Au NPs with proposed key parameters on different types of analyte. Amorphous carbon nanotubes (α-CNTs), copper (II) oxide (Cu_2O) and zinc sulphate ($Zn\ SO_4$) were arranged to be the analyte and the detection were examined optically via UV-Vis spectrophotometry.

1.2 Research Objectives

The objectives of this research are outlined as below;

1. To synthesis Au NPs via chemical reduction technique using monosodium glutamate salt (MSG) as reducing agent

2. To serve stabilized Au NPs through chitosan adsorption.

3. To examine the properties of Au NPs and chitosan capped Au NPs *via* several analytical technique comprise of UV-Visible Spectrophotometer (UV-Vis) and Transmission Electron Microscope (TEM).

4. To examine the capability of chitosan capped Au NPs in detection of amorphous carbon nanotubes (α-CNTs), copper (II) oxide (Cu_2O) and zinc sulphate ($Zn\ SO_4$) through optical characterization.

1.3 Scope of Thesis

Chapter One is organize to be the introductory part. The main objective are two folded, first, to synthesize Au NPs and chitosan capped Au NPs. While, the second ones revolve around on the studies of the key factor on the properties of Au NPs and chitosan capped Au NPs through characterization techniques.

Chapter Two prescribes a literature review of the synthesis method, material used and performance of materials in characterization enables of remanufacturing of Au NPs and chitosan capped Au NPs. The revolution of synthesis technique for Au NPs and chitosan capped Au NPs which caused the properties to altered is discussed briefly.

Chapter Three illustrates the experimental procedure of Au NPs and chitosan capped Au NPs production at finest condition. Water based synthesis of gold nanoparticles was carried out in single pot process through chemical reduction approach. The synthesis was further extended with chitosan adsorption on Au NPs surfaces within the same cycle process. Several characterizations comprise of Transmission Electron Microscopy (TEM) and UV-Visible spectrophotoscopy (UV-Vis) was also expounded in this chapter.

Chapter Four presents the experimental results for Au NPs and chitosan capped Au NPs synthesis. The results configured from TEM and UV-Vis are reviewed. The variable parameters which influence the size, behavior, morphology and size distribution of Au NPs are deliberated. In this section, the applications of chitosan capped Au NPs on detection of amorphous carbon nanotubes (α-CNTs), copper (II) oxide (Cu_2O) and zinc sulphate (Zn

SO_4). The behaviour of chitosan Au NPs upon detection of respective analyte was also examined. UV-Vis has been used to characterize the analytes detection by chitosan Au NPs.

Chapter Five reinforced the study as whole where conclusion and recommendations for future work are attached.

Chapter Two

LITERATURE REVIEW

CHAPTER TWO

Literature Review

2.1 Nanoparticles

Nanoparticles are defined as ultrafine particles in the size of nanometer range from 1 to 100nm. They are classified as nanocystals, polymeric, liposomal and solid lipid nanoparticles (Wu et al., 2011). Nanoparticles tend to have advanced capabilities in some area compared to bulky materials. They are hard, ductile at high temperatures, wear resistant, corrosion resistant, erosion resistant and are chemically active. Nanoparticles are made up of atoms or molecules similar to bulk material. However, the contraction of particles to nanometer range triggered the properties of the atoms and molecules itself, poles apart the bulk materials properties.

The simplified construction of nanoparticles has enhanced the activation of surface particles. The micronization of particles has also yielded increase in surface area to volume

ratio. The increase of surface area to volume ratio has become significant feature of nanoparticles that would lead to improvement in nanoparticles reaction and process. In clinical discipline, particles with high surface area to volume ratio give in better solubility and faster reaction rates (Hosokawa, 2007).

High surface area to volume ratio of nanoparticles has set off melting point depression. Bulk material has relatively higher melting point compared to nanoparticles. Nanda et al (2002) has employed empirical calculations based on Lindemanns criterion to demonstrate the relationship of melting temperature and cohesive energy. Surface atoms of nanoparticles tends to have less cohesive bonds. This leads atoms to freed themselves from solid phase with less energy. Hence, reduction in size has yielded reduction in melting temperature (Nanda et al., 2002). Liquid-drop model for the size-dependent melting of low-dimensional systems. A collection of reports has been represented emphasizing on size dependence melting properties with various material includes tin (Lai, 1996), aluminium (Sun et al., 2007), gold (Buffat et al., 1976), alumina supported Fe-C nanoparticles (Jiang,. 2007) and Ge nanoparticles (Lopeandia et al., 2007). The theoritical calculations of size dependence melting properties of nanoparticles basically calculated through Gibbs-Thomson equation. The classical thermodynamic analysis has been extended with different mechanisms and techniques comprising liquid-drop model (Peslherbe et al., 1999), Bond-order-length-strength (BOLS) model (Sun, 2007), Transmisson Electron Microscope (Marbeul et al., 1992) and nanocalorimeters (Vohra et al., 2011).

Metal nanoparticles such as Cu, Ag, Pb, Bi and In were reported to be additives in lubricating oils by dispersing the nanoparticulate into lubricating oils (Martin & Ohmae, 2008). While, Crooks et al (2000), reported dendrimer-encapsulated Pt Nanoparticles as

electrocatalysts in O_2 reduction. (Crooks et al., 2000). Noble metal nanoparticles which is gold and silver show a pronounced surface plasmon absorption and consistently competent in sequence analysis, electrochemical methods and protein bioassays (Gasparyan, 2009).

2.2 Au NPs

Gold which belongs to family of relic metal has established history with human civilizations back in 600 BC. The beauty of gold and its long lasting shine has become the lime light to human being (Pradeep & Anshup, 2009). On the other hand, gold in nanometer size were found to be invented and evolved along with bulk gold.

Au NPs have been exploited in the manufacturing of Lycurgus Cup back in 4th century during Roman times. The glass were found to be red in colour when exposed to light (Tait, 1991). The development of Au NPs continued with the discovery of purple solution of gold by Paracelsus in 15th century. The solution was called Aurum potable and has been exploited as rejuvenator to body. The first documentated literature for gold colloid was prepared by Antonii et al in 1618. Then, the properties of pink solution of gold have been explored by a German chemist in 1676 (Kunckels, 1676).

Recently, Au NPs gather suprising attention among researchers regards its unique optical, electric, electronic and catalytic properties. It has been utilised in multidisciplinary fields comprising physics, chemistry, biology and medicine. Their size tunable ability and localized surface plasmon resonance feature have brought Au NPs to various scope of research (Huang & El-Sayed, 2010; Turkevich et al., 1953; Narayanan & El-Sayed, 2005)

The most significance attribute of gold nanoparticles is the localized surface plasmon resonance phenomenon. Surface plasmon resonance defines as collective coherent oscillations of conduction electron of Au NPs as soon as exposed to incident light (Huang

& El-Sayed, 2010). As the nanoparticles confined to diameter, d which far less than wavelength of incident light, the polarization charges on the nanoparticles surface was builded up. These were contributed by movement of conduction electron in all phase once excited by light (Fu & Qiu, 2011). The plasmon phenomenon serves as restoring force in allowing resonance to occur at specific frequency. The dipole plasmon frequency was the frequency where the electron oscillates resonantly and responses phase lagging for $\pi/2$ in external driving field (Fu & Qiu, 2011).

For the past decade, researchers have made the most of Au NPs in a range of applications (Daniel & Astruc, 2004). In electronics, Au NPs have been patterned to be conductors in all sorts of electronic devices such as electronic chip (Huang et al., 2003). Au NPs have showed competency in medicinal field. Correspondingly, their applications may be classified into five groups; labeling (Boisselier, 2009), sensing (Soonwo, 2005), diagnostics (Huang, 2010), delivery (Ghosh et al., 2008) and heating (Pissuwan et al., 2006). Moreover, Au NPs have been reported to be efficient catalyst (Burato et al 2005, Miyamura et al 2007, Prati & Rossi 1998). They are favourable due to their chemoselectivity and ability to amplify electrochemical reactions (Endo, 2009).

2.3 Synthesis of Au NPs

There are two routes to manufacture metal nanoparticles involving either top down or bottom up approach. In top down method, bulk material was discarded according to new design of desired structures. While bottom up method are basically enlargement of reduced ions to enormous structures. Bottom up route comprises of a variety of techniques namely, microemulsion, reversed micelles, seeding growth, sonochemistry, photochemistry, radiolysis, direct chemical reduction and others (Roos et al. 1999; Freeman et al. 1996; Cao et al. 2005)

In practice, bottom up route hold advantage over top down route. Top down has to undergo massive shed of bulk material before desired nanostructures obtained (Eustis et al., (2005). Furthermore, nanoparticles manufactured by this route are yield to high surface defects. These surface imperfections have impinge on thermodynamic equilibrium. On the other hand, bottom up method allows the synthesis of monodispersity nanoparticles with less surface defects (Kreibig et al., 1995).

The bottom up routes may be divided into two approachs of synthesis of Au NPs via synthesis in water and in non-polar organic solvents. Water based gold nanoparticles synthesis have comparable advantages over organic solution based synthesis of Au NPs. The synthesis of gold nanoparticles in water can be done in one-pot process. While, the reduction and capping of Au NPs in organic solution requires multi step operations including a phase transfer. Moreover, the main advantage of water based synthesis is surface functionalization and bioconjugation with antibodies can be effortlessly achieved,

since organic environment is not suitable for biological applications (Rao et al., 2004).

Figure 2.1 illustrates the formation of Au NPs starting with the reduction of gold chloride. The electron from the oxidized amino group of MSG transferred to gold ion leads to formation of zerovalents gold (Wangoo et al., 2008). Consecutively, the zerovalent gold nucleates and inflates to form Au NPs. The layer of the oxidized product on the gold surface stabilizes Au NPs electrostatically (Wangoo et al., 2008). The single electron transfer was further discussed by Daniel et al. (2004). Single electron transfer was observed with a phenomenon called Coulomb blockades in Differential pulse voltammetry (DPV) where the capacitance, C is small enough and contributes to high the electrostatic energy, $E_{el} = e^2/2C$ (Daniel et al., 2004).

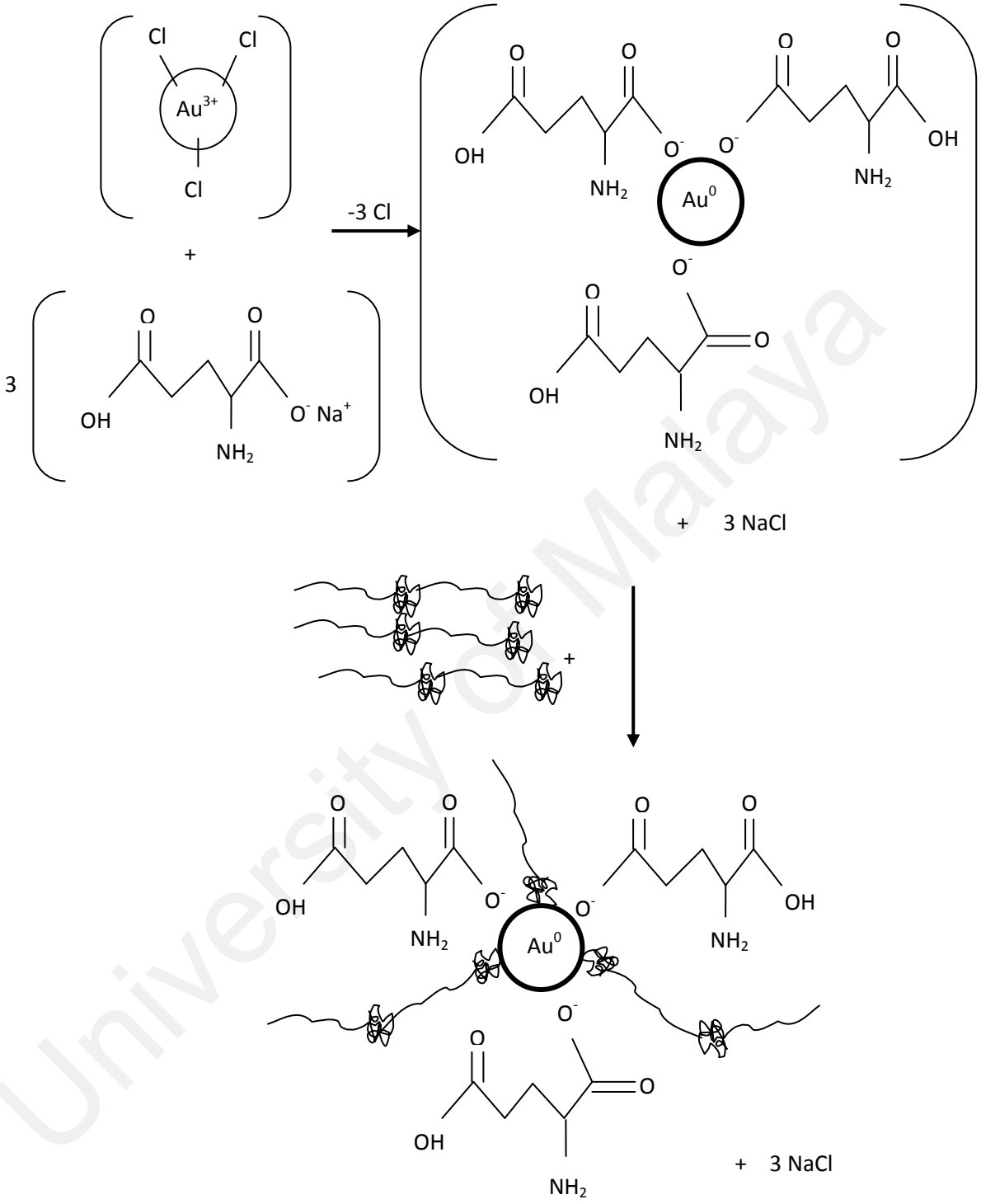

Figure. 2.1 Schematic structural diagram of reduction of gold precursors by MSG and capping the gold particle surfaces with chitosan (Wangoo et al., 2008).

2.4 Chitosan capped gold nanoparticles

Au NPs have tendency to agglomerate due to van der Waals interactions as surface energy increase (Hamaker, 1937). The necessity of capping material to Au NPs is to counteract the van der Waals interaction and imparting stability by decreasing the surface energy. There are also demand in providing readily surface of Au NPs for functionalization and bioconjugation (Kumar, 2007). Capping agent functioned as a linkage between Au NPs and macromolecule, either by developing negatively charged surface or by derivatizing hydrophobic domains onto Au NPs surface (Songjun et al., 2011). Au NPs are been able to become stable by electrostatic and steric stabilization. Electrostatic stabilization would be initiated by adsorbing ionic substances onto Au NPs (Koetz & Kosmella, 2007). While steric hindrance has instigated as hydrocarbons chain anchored on the surface of Au NPs (Zhou et al., 2009). Various capping agent with their respective active molecule groups comprising amino ($-NH_2$), carboxylic acid (-COOH), mercapto (-SH) and cyano (-CN) have been employed as capping agent to Au NPs (Pradeep & Anshup, 2009). These surface active groups have high affinity to Au NPs and believe to integrate with Au NPs effectively (Teranishi et al., 1998).

Chitosan are among capping agent which have successfully protected the Au NPs from agglomeration. Chitosan has become cationic polymer in acidic media as the protonation of (NH_2) groups. The multi-sites of free amines allow chitosan to anchor on the surface of nanoparticles more competent ahead of others (Guibal, 2004). The stabilization mechanism was further discussed by Napper (1983) in which the hydrophobic end of chitosan has incorporated with the gold particles surface either by physi-sorption or chemi-sorption. On

the other hand, the hydrophilic end of chitosan imparts the steric stabilization. Au NPs capped with chitosan have been reported by Roshdi et al (2011) as catalyst for reduction of 4-nitrophenol by $NaBH_4$. Chitosan capped Au NPs has recorded high catalytic activity compared to Au NPs capped with sodium citrate and cetyltrimethylammonium bromide (CTAB) (Roshdi et al., 2011).

Figure 2.2 showed the monomer structure of chitosan polymer. Chitosan is issoluble in water but readily soluble in dilute acidic solutions below pH 6.0. There are various organic acids used as solvents for chitosan includes formic acid, acetic acid, lactic acid, hydrochloric acid and nitric acid.

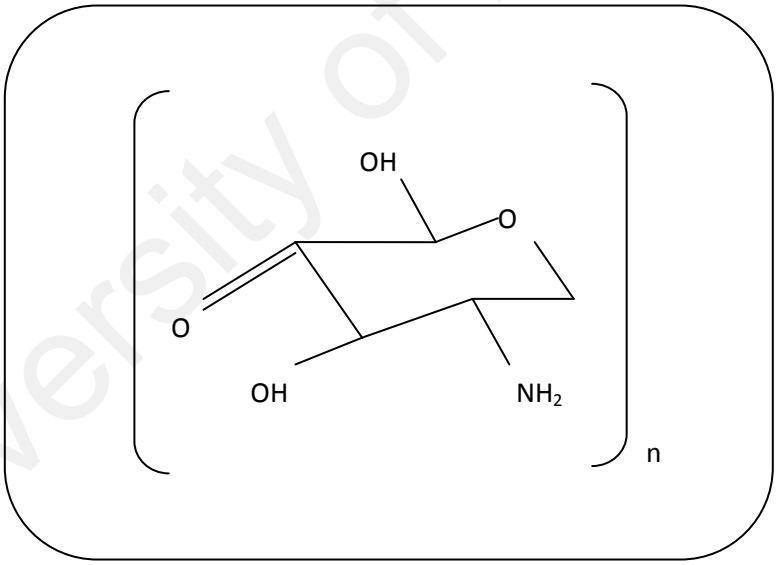

Figure 2.2: The monomer units for chitosan, whereby value of n depends in the molecular weight of chitosan

2.5 The size dependence properties of Au NPs

The size dependence properties of spherical nanoparticles were explained by Mie (1908). He has solved an electrodynamic calculation of small spheres interacted with electromagnetic wave through the Maxwell equation. The partial waves of multipole oscillations for the extinction cross-section of nanoparticles were considered and the following expression of extinction cross-section, σ_{ext} and scattering cross-section, σ_{sca} were established (Mie, 1908). The surface plasmon resonance was initiated by dipolar oscillations of electrons with period of *T*. The electron has been subjected to a restoring force that has been contributed by variation of surface charges where positive charges represent the lacking of electron cloud while negative charges corresponded to concentrated cloud of electron (Link & El-Sayed, 2000; Moores & Goettmann, 2006).

$$\sigma_{ext} = \frac{2\pi}{|k|^2} \sum_{L=1}^{\infty} (2L+1)\,\mathrm{Re}\,(a_L + b_L) \tag{2.1}$$

$$\sigma_{sca} = \frac{2\pi}{|k|^2} \sum_{L=1}^{\infty} (2L+1)\left(|a_L|^2 + |b_L|^2\right) \tag{2.2}$$

Absorption cross-section, $\sigma_{abs} = \sigma_{ext} - \sigma_{sca}$ and a_L, b_L represented as;

$$a_L = \frac{m\psi_L(mx)\psi_L'(x) - \psi_L'(mx)\psi_L(x)}{m\psi_L(mx)\eta_L'(x) - \psi_L'(mx)\eta_L(x)},$$

$$b_L = \frac{m\psi_L(mx)\psi_L^{'}(x) - \psi_L^{'}(mx)\psi_L(x)}{m\psi_L(mx)\eta_L^{'}(x) - \psi_L^{'}(mx)\eta_L(x)}$$

Where;

$m = n/n_m$, n is the complex refractive index of the particle and n_m is the real refraction index of the surrounding medium,

k is the wave-vector,

$x = |k|r$, r is the radius of the nanoparticle,

ψ_L and η_L are the Ricatti-Bessel cylindrical functions,

L=1 is the summation index of dipole oscillations.

The theory was then reduced to dipole approximation relationship as in equation (2.3) for nanoparticles which is much smaller than wavelength of light $(2r < \lambda_{\max}/10)$.

$$\sigma_{ext} = \frac{24\pi^2 R^3 \varepsilon_m^{2/3}}{\lambda} \frac{\varepsilon_2}{(\varepsilon_1 + 2\varepsilon_m)^2 + \varepsilon_2{}^2} \qquad (2.3)$$

Where;

R = radius of the particles

λ = wavelength of surface plasmon resonance

ε_m = the dielectric function of surrounding medium

$\varepsilon = \varepsilon_1 + i\varepsilon_2$ = the dielectric function of the material

The above expressions will be $\varepsilon_1 = -2\varepsilon_m$ at the surface plasmon resonance conditions. From equation 2.3, the relationship of radius of the resultant particles with the position of surface palsmon resonance wavelength may be observed. Tiggesbaumker et al (1992) have proved the relationship in an experiment where the blue shift perceived as the nanoparticles

size decreased.

2.6 Theoretical studies of Beer Lambert Law and Benesi-Hildebrand method

A mathematical approach called the Benesi-Hildebrand method allows the determination of equilibrium constant by simulating the optical characterization (Wang & Yu, 2007). The simplified reaction of chitosan-conjugated Au NPs is as follows;

$$AuNp + chitosan \rightarrow AuNp - chitosan$$

$$K_{eq} \approx \frac{[AuNp\ complex]}{[AuNp][chitosan]} \tag{2.4}$$

The equilibrium constant, K_{eq} is derived from the above reaction as in Equation (2.4). The derivation is further extended considering uncoordinated Au NPs and chitosan as in Equation (2.5).

$$K_{eq} \approx \frac{[AuNp\ complex]}{\{[AuNp]_0 - [chitosan]\}\ \{[chitosan]_0 - [AuNp]\}} \tag{2.5}$$

Where;

$[AuNp]_0 = total\ AuNp\ (coordinated\ and\ uncoordinated) = [AuNp] + [AuNp\ complex]$

$[chitosan]_0 = total\ chitosan\ (coordinated\ and\ uncoordinated) = [chitosan] + [AuNp\ complex]$

If $[AuNp]_0 >> [chitosan]_0$, then $\{[chitosan]_0 - [AuNp\ complex] \approx [chitosan]_0$, the equation (2.5) will be transformed as below;

$$K_{eq} \approx \frac{[AuNp\ complex]}{\{[AuNp]_0 - [AuNp\ complex]\}[chitosan]_0} \quad (2.6)$$

Hence,

$$\frac{1}{K_{eq}} \approx \frac{[AuNp]_0[chitosan]_0}{[AuNp\ complex]} - [chitosan]_0$$

$$\frac{1}{K_{eq}[chitosan]_0} \approx \frac{[AuNp]_0}{[AuNp\ complex]} - 1$$

$$\frac{1}{K_{eq}[chitosan]_0} + 1 \approx \frac{[AuNp]}{[AuNp\ complex]}$$

$$\frac{[AuNp]}{[AuNp\ complex]} \approx \frac{1}{K_{eq}[chitosan]} + 1 \quad (2.7)$$

According to Beer-Lambert Law, the relationship of absorbance and light intensities is as in Equation (2.8) (Benesi and Hildebrand 1949)

$$\Delta A = \log \frac{I_o}{I} = \varepsilon_c\, x\, \ell \quad (2.8)$$

$$x = \frac{\Delta A}{\varepsilon_c \ell}$$

where ΔA= delta absorbance between two samples, I_o = light intensity passing through reference cell, I = light intensity passing through sample cell, ε_c = extinction coefficient of Au NPs complex, ℓ = sample cell length and x = concentration of Au NPs complex. When the intensity of incident light irradiates sample cell, I is less than intensity of incident light

passing through the reference cell, $I_{o,}$ the particles absorbed light (Clark, 2007). Beer-Lambert Equation was plugged into Equation (2.7) as

$$\frac{[AuNp]_0 \, \varepsilon c \ell}{\Delta A} \approx \frac{1}{K_{eq} [chitosan]_0} + 1 \qquad (2.9)$$

And the final expression as below;

$$\frac{1}{\Delta A} \approx \frac{1}{K_{eq} [AuNp]_0 \, \varepsilon c \, \ell} \left(\frac{1}{[chitosan]_0} \right) + \frac{1}{[AuNp]_0 \varepsilon c \ell}$$

(2.10)

At equilibrium, relationship of equilibrium constant and Gibbs free energy can be expressed as in Equation (2.) (Wilson and Beezer, 2003). Where ΔG= Gibbs free energy, R= gas constant, T= ambient temperature and K_{eq} is the equilibrium constant. The determination of equilibrium constant initiates the exploration of thermodynamic matter of the newly made Au NPs complex. The Gibbs free energy give an overview of the energy barrier a particle has to overcome before it re-agglomerate (Blaber, 2002).

$$\Delta G = - RT \ln K_{eq} \qquad (2.11)$$

Where;

ΔG= Gibbs free energy,

R= gas constant,

T= ambient temperature and

K_{eq} is the equilibrium constant

2.7 Effect of amorphous-carbon nanotube (α-CNTs)s, copper (II) oxides and zinc sulphate to chitosan capped gold nanoparticles

Carbon nanotubes and chitosan have been found to be coupled and synthesis together in several research. Jia et al. (2008) have coupled chitosan, amourphous carbon nanotubes and gold in a electrode for elctrochemical cyctosensing. Carbon nanotubes are also prevalent same as chitosan in biological applications. Carbon nanotubes have strong influence in cancer therapy, neuronal living networks, act as delivery agent for immunostimulants and vaccines and biosensor and bio-interfacial materials (Pastorin, 2011).

Chitosan as chelating agent has been extensively utilized together with Au NPs as heavy metal ions sensor (Sugunan et al., 2005). Au NPs capped with chitosan successfully captured the metal ions by showing signs of agglomeration. The source of Cu^{2+} and Zn^{2+} ions were obtained by preparation of copper sulphate and zinc acetate. The ease of metal ion detection by chitosan has made the heavy metal ions sensor as point of reference for our work. Besides, Yap et al. (2011) have additionally showed the optical properties of chitosan film towards the copper ion detection through surface plasmon resonance technique. The copper ion detection were highlighted by the decreased in resonance angle shift of SPR curves for copper ion solutions (10–100 ppm) being in contact with gold/cross-linked chitosan layer.

2.8 Materials and Instrumentations

2.8.1 Gold (III) Chloride

Gold (III) chloride, traditionally called auric chloride, is the chemical compound with the formula $AuCl_3$. The Roman numerals in the name indicate that the gold has an oxidation state of +3, which is common for gold in its compounds. Gold (III) chloride is very hygroscopic and highly soluble in water and ethanol. It decomposes above 160 °C or in light. $AuCl_3$ exists as a dimer both as a solid and as a vapour at low temperatures in which each gold center is square planar. The structure is illustrated in Figure 2.3. $AuCl_3$ has high oxidation state reflects the covalent bonding between the molecules. In addition, $AuCl_3$ has high electronegativity compared to the other metal.

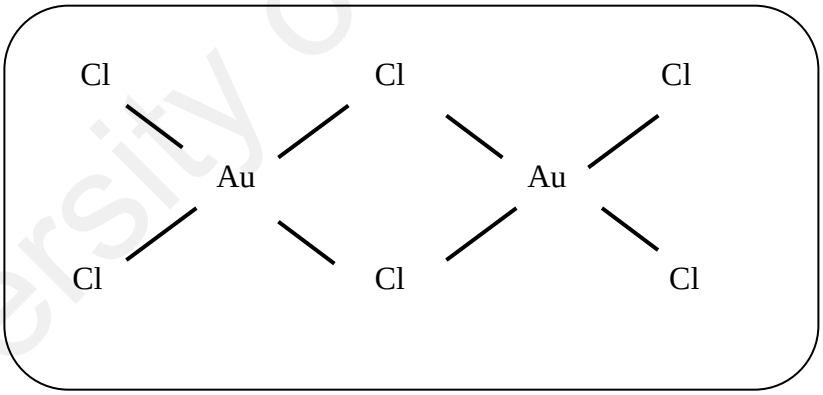

Figure 2.3 :The arrangement of Gold (III) Chloride

2.8.2 Monosodium Glutamate (MSG)

Monosodium glutamate, also known as sodium glutamate and MSG, is a sodium salt of glutamic acid, a naturally occurring non-essential amino acid. It is a white crystalline substance soluble in water and alcohol; practically odorless. MSG is used to intensify flavours of foods. It is produced by a bacterial fermentation process with starch or molasses as carbon sources and ammonium salts as nitrogen sources (Steffen process). From 1909 to the mid-1960s, MSG was prepared by the hydrolysis of wheat gluten, which is roughly 25% glutamic acid. MSG is a stable colourless solid that is degraded by strong oxidizing agents. It exists as a pair of mirror image stereoisomers.

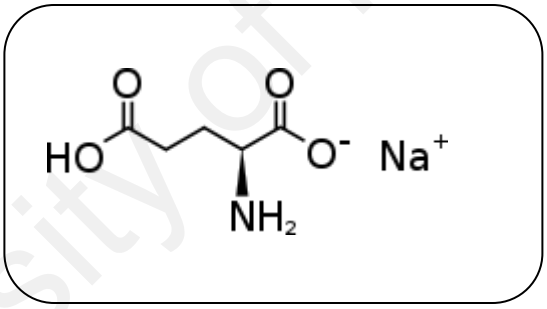

Figure 2.4 The structure of Na salt of L-glutamic acid

2.8.3 Chitosan

Chitosan is a linear polysaccharide composed of randomly distributed -(1-4)-linked D-glucosamine (deacetylated unit) and N-acetyl-D-glucosamine (acetylated unit). Chitosan is produced commercially by deacetylation of chitin, which is the structural element in the exoskeleton of crustaceans (crabs, shrimp, etc.). It has a number of commercial uses in agriculture, water and waste treatment, food and beverages, cosmetics and toiletries and biopharmaceutics (Rinaudo, 2006).

Chitosan has high percentage of nitrogen (6.89%) compared to synthetically substituted cellulose (1.25%). This feature turned out chitosan as a chelating agent (Rinaudo, 2006). Many previous works on metal capture and removal by chitosan have been reported involving metal ions of Hg^{+} ,Hg^{2+},Cd^{2+} , Cu^{2+} , Ni^{2+}, Zn^{2+} and Cr(III) (Rinaudo, 2006).

Chapter Three

EXPERIMENTAL TECHNIQUE

CHAPTER THREE

Experimental Technique

3.1 Materials used

The chemicals utilized were among of analytical reagent grade without purification. Gold (III) chloride ($AuCl_3$) (Acros Organics) was used as Au source. Monosodium glutamate acid (MSG) was chosen to be the reducing agent. Chitosan flakes (MW 8000) were further processed to be soluble stabilizer. Acetic acid was used to alter chitosan solubility in water. Distilled water was used as main solvent in the preparation of Au NPs and chitosan capped Au NPs. Amorphous carbon nanotubes (α-CNTs), copper (II) oxide (Cu_2O) (Sigma Aldrich), zinc sulphate (Zn SO_4) (Sigma Aldrich) were choose to be the analyte which represent carbon nanotubes, oxides and sulphate.

3.2 Synthesis Introduction

In this work, the ratio of gold precursors to reducing agent were according to Sugunan and Dutta (1999) where the small molar ratio of gold chloride to MSG was used. The higher molar concentration of reducing agent was determined in order to investigate the size trends and behavior of Au NPs and chitosan capped Au NPs. Duration of the synthesis was also varied to study the growth of Au NPs. The weight ratio of chitosan was varied in order to investigate the optimum concentration of stabilizer.

3.2.1 Au NPs Synthesis Procedure

Au NPs were produced by reduction of $AuCl_3$ by MSG in a one pot synthesis. The process are simplified in Figure 3.1 (a) in which 2 mL of 5 mM gold (III) chloride solution and 3 mL of 50 mM monosodium glutamate (MSG) solution was poured in 100 mL distilled water and heated up to 160 ^{o}C. The solution was stirred along the process for 1 hour and further stirred for 1 min until no changes of colour observed. The temperature was determined in conjuction to the thermal decomposition of gold (III) chloride. The colour of the solution turned from transparent to pale purple and followed by intensed purple upon the development of Au NPs indicating the presence of zerovalent gold colloids from reduction of Au^{3+} ions by MSG. The samples were further characterized by TEM and UV-Vis spectrophotometer. The experimental details are listed in Table 3.1. For the stability testing, Au NPs reduced with different concentration of MSG, 100 mM, 150 mM, 200 mM, 250 mM and 300 mM were left under ambient temperature for 1 month. The samples were then characterized by UV-Vis.

Table 3.1: Experimental details of Au NPs synthesis parameters

Sample name	Concentration of Gold chloride solution (mM)	Weight of Gold chloride powder (g) dissolve in 100mL of water	Concentration of Monosodium glutamate (MSG) solution (mM)	Weight of Monosodium glutamate (MSG) powder (g) dissolve in 50 mL of water
Au NPs reduced with 50 mM of MSG	5	0.1517	50	0.4679
Au NPs reduced with 100 mM of MSG	5	0.1517	100	0.9357
Au NPs reduced with 150 mM of MSG	5	0.1517	150	1.4036
Au NPs reduced with 200 mM of MSG	5	0.1517	200	1.8714
Au NPs reduced with 250 mM of MSG	5	0.1517	250	2.3393
Au NPs reduced with 300 mM of MSG	5	0.1517	300	2.8072

3.2.2 Chitosan capped Au NPs Synthesis Procedure

Various amount of chitosan flakes were grounded using heavy duty blender until fine powder obtained. The grounded powder was then dissolved into 1% of acetic acid, heated at 50 ^{o}C and stirred for 24 hour. 990 μL of chitosan solution is poured into the Au NPs solution as produced in 3.1.1. The solution was transformed to dark purple upon addition of chitosan solution. The newly made solution was set under stirring for 15 minutes without any heat. The steps were repeated with Au NPs reduced with different concentration of MSG, in examples, 100 mM, 150 mM, 200 mM, 250 mM and 300 mM. The samples were then characterized by TEM and UV-Vis. The procedure was illustrated in a diagram in Fig. 3.1 (b). For the stability testing, Au NPs capped with chitosan reduced with different concentration of MSG, 100 mM, 150 mM, 200 mM, 250 mM and 300 mM were left under ambient temperature for 1 month. The samples were then characterized by UV-Vis.

3.2.3 Amourphous Carbon Nanotubes - Chitosan Capped Au NPs synthesis procedure

The synthesis procedure is followed Tan (2011). The procedure was instigate with mixture of 8 mL of ethyl alcohol (90%), 4.2 g of $NaBH_4$ (99.99%) and 15 mL of 1M NaOH in a 25 mL flask. The solution was further stirred for next 45 minutes before transferred to a Parr reactor with capacity of 200 mL. The reactor was heated inside a furnace up to 200 ^{o}C and hold for 2 hours under scaled condition. The Parr reactor was allowed to cool to ambient temperature and the precipitate were washed thoroughly with alcohol and deionised water. The precipitate was then dried in the vacuum oven.

The as-synthesized amorphous CNTs powder was added to chitosan capped Au NPs solution (1 g of chitosan powder and 100 mM of MSG) and the samples were further characterized by UV-Vis spectrophotometer.

3.2.4 Copper Oxide - Chitosan Capped Au NPs Synthesis Procedure

Various amount 5g of copper oxide powder was added to chitosan capped Au NPs solution (1 g of chitosan powder and 100 mM of MSG) and the samples were further characterized by UV-Vis spectrophotometer.

3.2.5 Zinc Sulphate - Chitosan Capped Au NPs Synthesis Procedure

Various amount of zinc sulphate powder was added to chitosan capped Au NPs solution (1 g of chitosan powder and 100 mM of MSG) and the samples were further characterized by UV-Vis spectrophotometer.

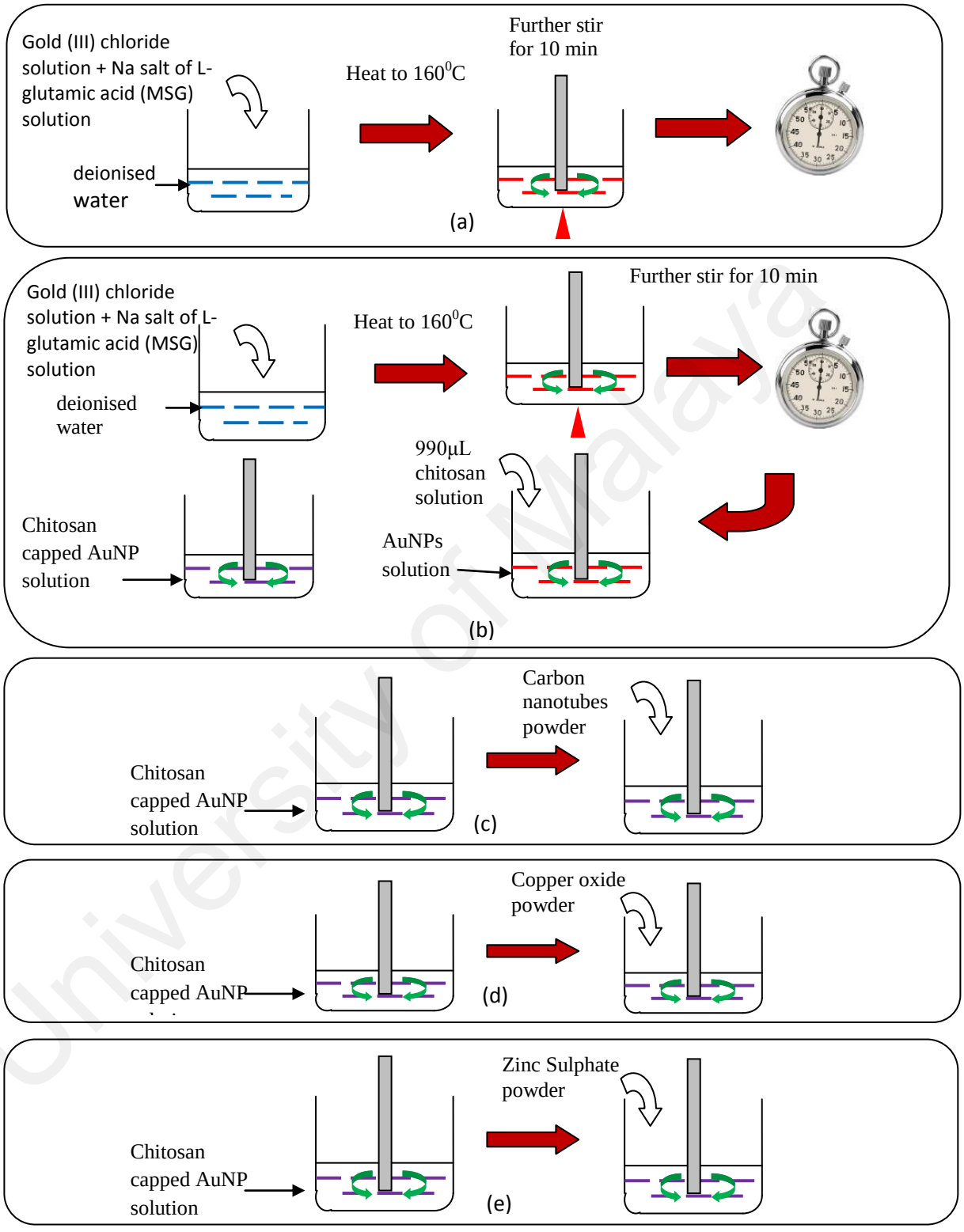

Figure 3.1: The preparation procedure of (a) Au NPs, (b) chitosan capped Au NPs (c) Carbon nanotubes detection by chitosan capped Au NPs, (d) Copper (II) Oxide detection by chitosan Au NPs, (e) Zinc sulphate based material detection by chitosan capped Au NPs

3.3 Characterization techniques

The properties of gold nanoparticles and chitosan capped Au NPs were investigated by several characterization techniques. The optical characteristics of the samples were studied by Cary 50 Scan UV-Visible Spectrophotometer. The quantum mechanics and thermodynamic stability were furthered simulated via the optical characterization. The size distribution and morphology of the particles were monitored using LEO 733 Libra transmission electron microscope (TEM).

3.3.1 Transmission electron microscopy (TEM) Analysis and Sample preparation

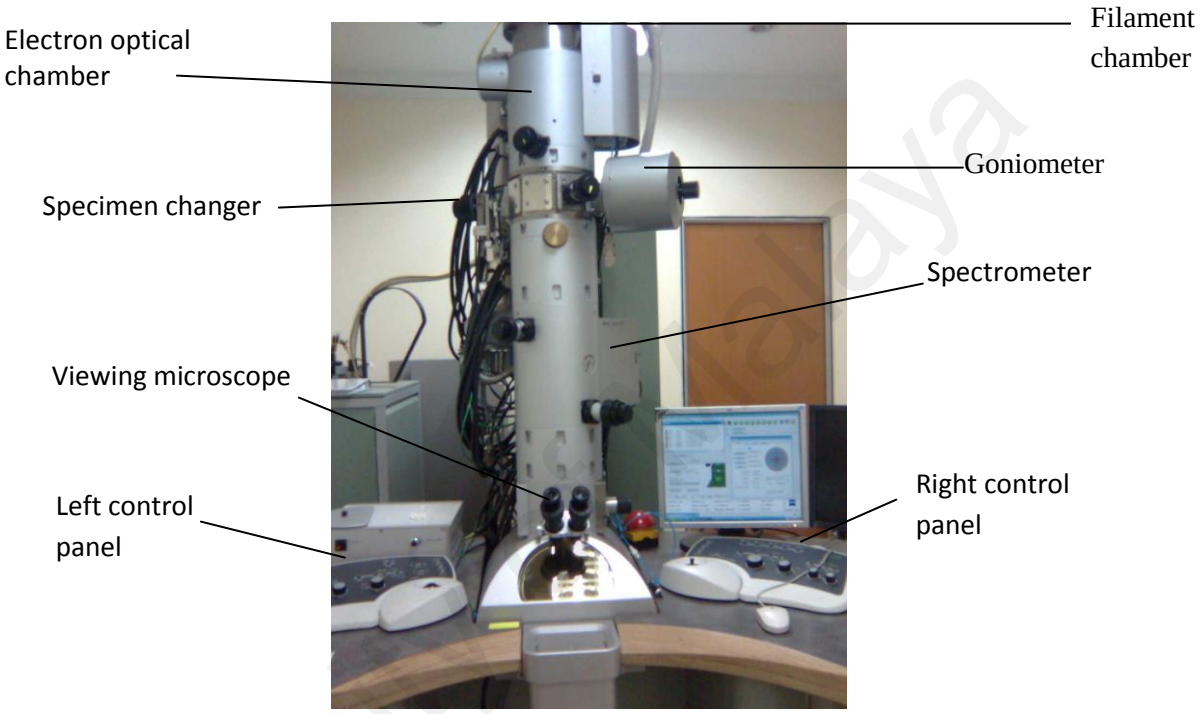

Figure 3.2: Transmission Electron Microscope

The surface and size distribution of Au NPs and chitosan capped Au NPs were determined under LEO LIBRA transmission electron microscope operated at 200 kV. Figure 3.2 shows the Transmission Electron Microscope used in this research. In the sample preparation, samples must remain stable and electron transparency when undergoes extreme condition throughout the analysis which includes extreme heat generated by the electron beam and high vacuum.

The Au NPs and chitosan capped Au NPs samples were dispersed in ethanol. Then, the samples were allowed to sonicated in ultrasonic bath for 6 hours. The sonification process is done in order to ensure the dispersion of the solution. A few drops of samples solution were allowed to dry on carbon coated grid for almost 3 days. The drying period is most essential in order to prevent any waterlogged on the grid. The dried samples grid will permit clearer image without any layer of water.

The grid was further inserted in the duo sample holder in the microscope tower. In advance, the filament and electron chamber are ensured to be under vacuum condition. The minimum number of four cycles of vacuum pumping was regulated before insertion of particles to the chamber. The microscope was systemized to operate at pressure of 10^7 torr. The filament was heated by saturation current of 113 μA. The power supply was turned off after the operation current and pressure were deliberated to set up the acceleration voltage at 200 kV. The aperture was selected for image processing. Once an image formed on the screen, the sample was magnified and focused with specific magnification. Then, the selected area was captured on high resolution built in camera.

The particles size measurements were performed with KONTRON 400 (Zeiss Kontron), a particles size analyzer software package. The scale and the threshold was set to a uniform value for the whole image, the “Measure arbitratory distance" feature was used to measure 100 non touching particles diameter. A table of particle diameter values was generated and exported to Microsoft Excel, where histogram plotting was performed.

3.3.2 Ultra Violet Visible (UV-Vis) Analysis and Sample preparation

Cary 50 UV-Visible spectrophotometer was employed to measure the percentage of UV-Vis radiation that is absorbed by Au NPs at specific wavelength. Figure 3.6 shows the UV-Visible spectrophotometer used in this research. The wavelength range for the equipment is from 200 to 800 nm. Ultraviolet (200-400 nm) and visible (400-800 nm) radiation are commence at shorter wavelength which corresponds to high frequency and high energy. The range of wavelength from 400 to 700 nm was set up for this research. The scan rate was fixed at 600.0 nm (min^{-1}) with data interval of 1.0 nm. The scan software used in the instrument was Cary 50 version 3.0(182). The baseline correction was establish as the baseline type in which water was identified as reference for both gold nanoparticles and chitosan capped Au NPs samples solution. In advance, the sample was sonicated in ultrasonic bath for 1 minutes in deionized distilled water. The plot recorded for all samples are disclosed and further discussed in Chapter 5.

Figure 3.6: UV-Visible spectrophotometer

Chapter Four

RESULTS AND DISCUSSION

CHAPTER FOUR

Results and Discussion

4.1 Transmission Electron Microscopy (TEM) studies

Figure 4.1 shows the TEM image of Au NPs before and after capping with chitosan. The uncapped Au NPs are in spherical shape and closer among themselves. Meanwhile, Figure 4.2 shows the Au NPs are much dispersed after capping with chitosan. Chitosan has resembles a spider web and hinder the agglomeration between the particles.

Figure 4.3 shows the particles size distribution of Au NPs before and after capping with chitosan. Both figures shows narrow particles size distribution with the most probable size of Au NPs are in the range of 16 to 18 nm. It can be observed that chitosan retain the size of Au NPs and stabilize the particles through a spider web.

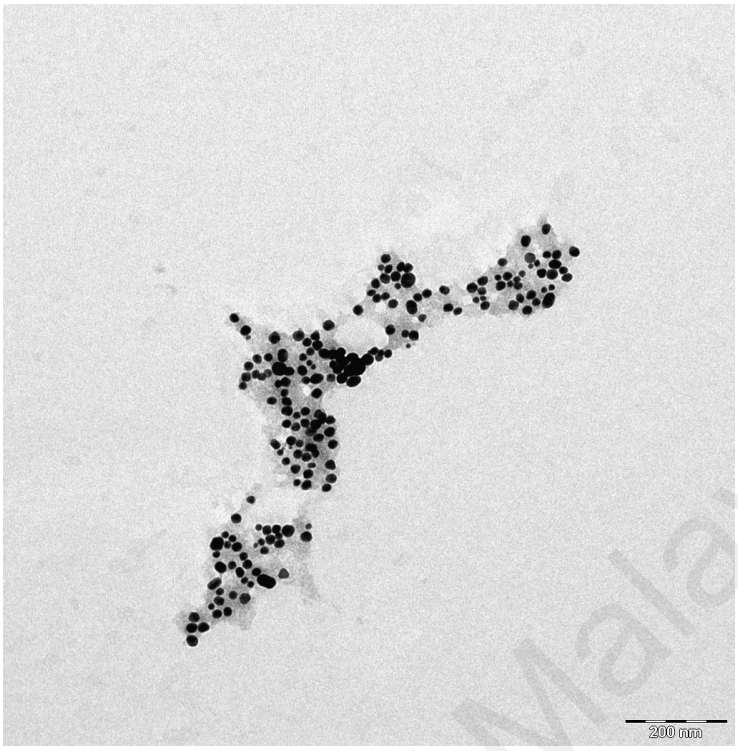

Figure. 4.1: TEM images of Au NPs before capping with chitosan

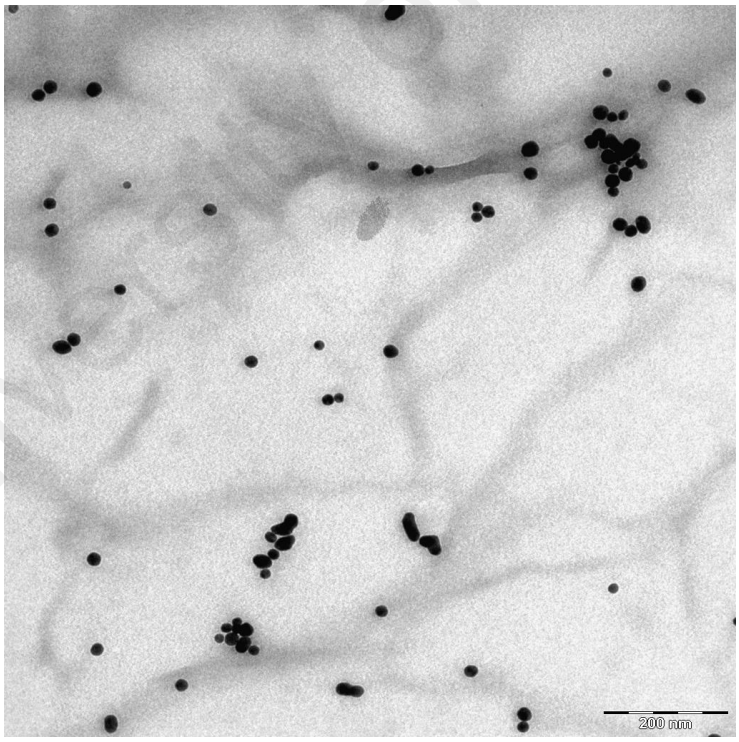

Figure. 4.2 : TEM images of Au NPs after capping with chitosan

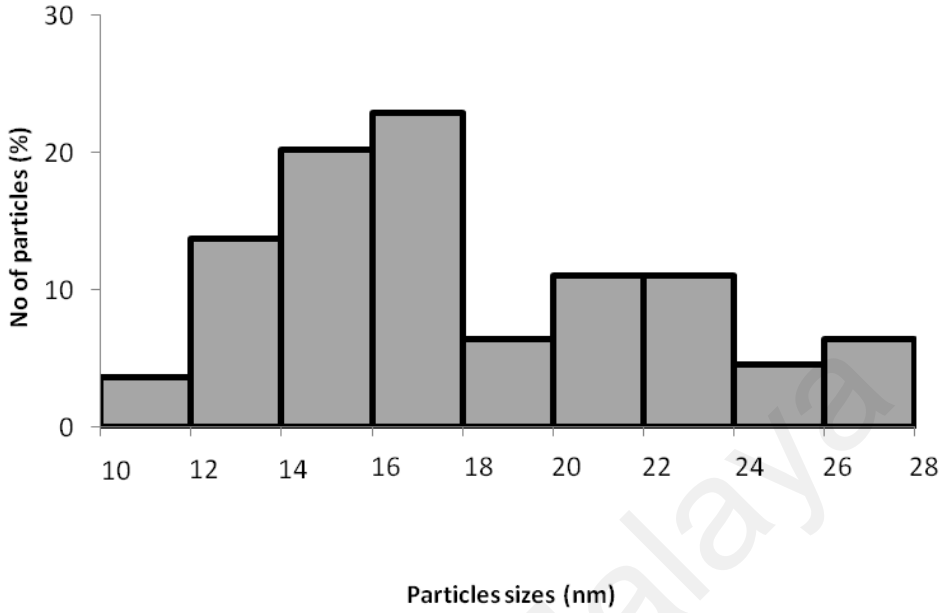

(a) Au NPs

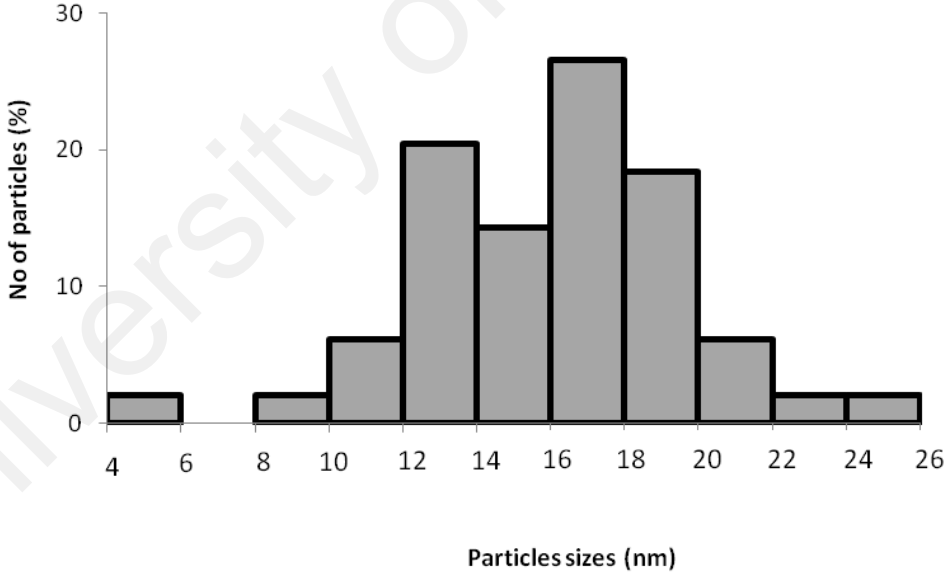

(b) Chitosan capped Au NPs

Figure 4.3: Particle size distribution of Au NPs (a) before capping, (b) after capping with chitosan

4.2 Optical studies of UV-Visible spectrophotometer studies

Figure 4.4 shows the UV-Vis spectra for Au NPs before and after capping with chitosan. A departure has been spotted for chitosan capped AuNPs absorption spectra due to changes in dielectric constant of reaction medium. Figure 4.5 shows the absorption spectra of non-capping Au NPs at various concentration of reducing agent. It shows that the SPR bands are blue shifted from 532 nm to 523 nm as the concentration of reducing agent increases. This indicates that the size of the particles decreases as the concentration of the reductant increased. Table 4.1 summarizes the results.

Equation (4.1) shows the relation between the SPR peak, particles size and concentration of reductant (Sugunan et al., 1999).

$$AuCl_3 + (x+3)\, NaC_5H_8O_4N \longrightarrow Au\ 3[C_5H_8O_4\,N]^- + 3NaCl + x[C_5H_8O_4\,N]^- + xNa^+ \qquad (4.1)$$

where (x+3) is the molar ratio of MSG to $AuCl_3$. According to the above equation, three molecule of MSG are required to transfer their electrons to gold (III) chloride molecule in order to reduce them. These verify that the concentration of MSG should be three times more than concentration of gold precursors to enhance homogeneity of particles. Therefore, the higher amount of MSG leads to smaller particles of gold since there were sufficient amount of MSG to reduce gold precursors completely. Simultaneously, the layer of oxidized product on the gold surface stabilizes the particles from growing larger.

Antoneiti (2003) has explained the relationship between absorption intensity and

concentration of reducing agent in which absorption intensity increases as concentration of reducing agent increases. The absorption spectra in Figure 4.5 show inverse proportionality of absorption intensity and concentration of reducing agent. The absorption intensities for uncapped Au NPs are constant before it started declined at concentration of 300 mM. The gold particles reduced by 300 mM of MSG shows smallest FWHM and λ_{max} among the rest but the absorption intensity are not as expected. This probably causes by the high concentration of excess MSG and Na + ions in solution which constricts the absorption of light by the particles.

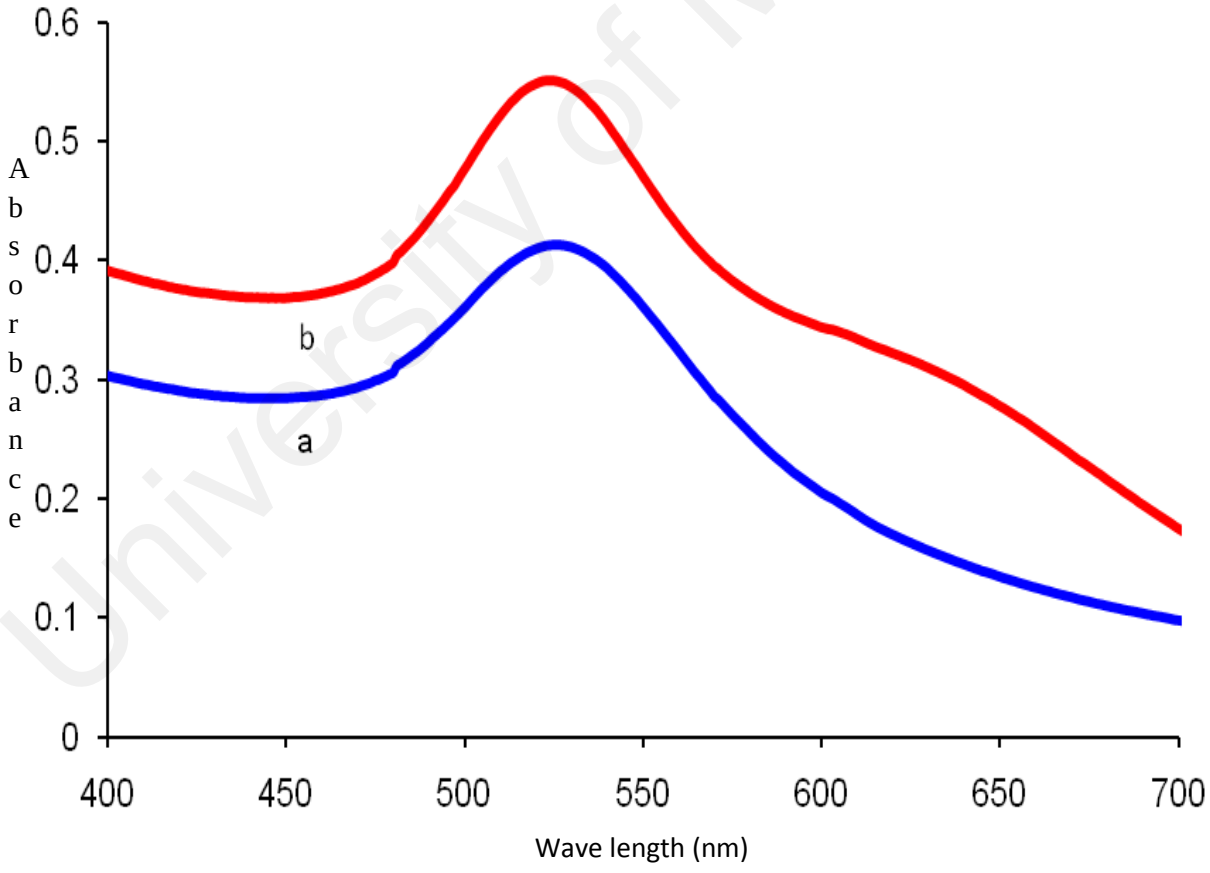

Figure. 4.4: Absorption spectra of Au NPs (a) before capping, (b) after capping with chitosan

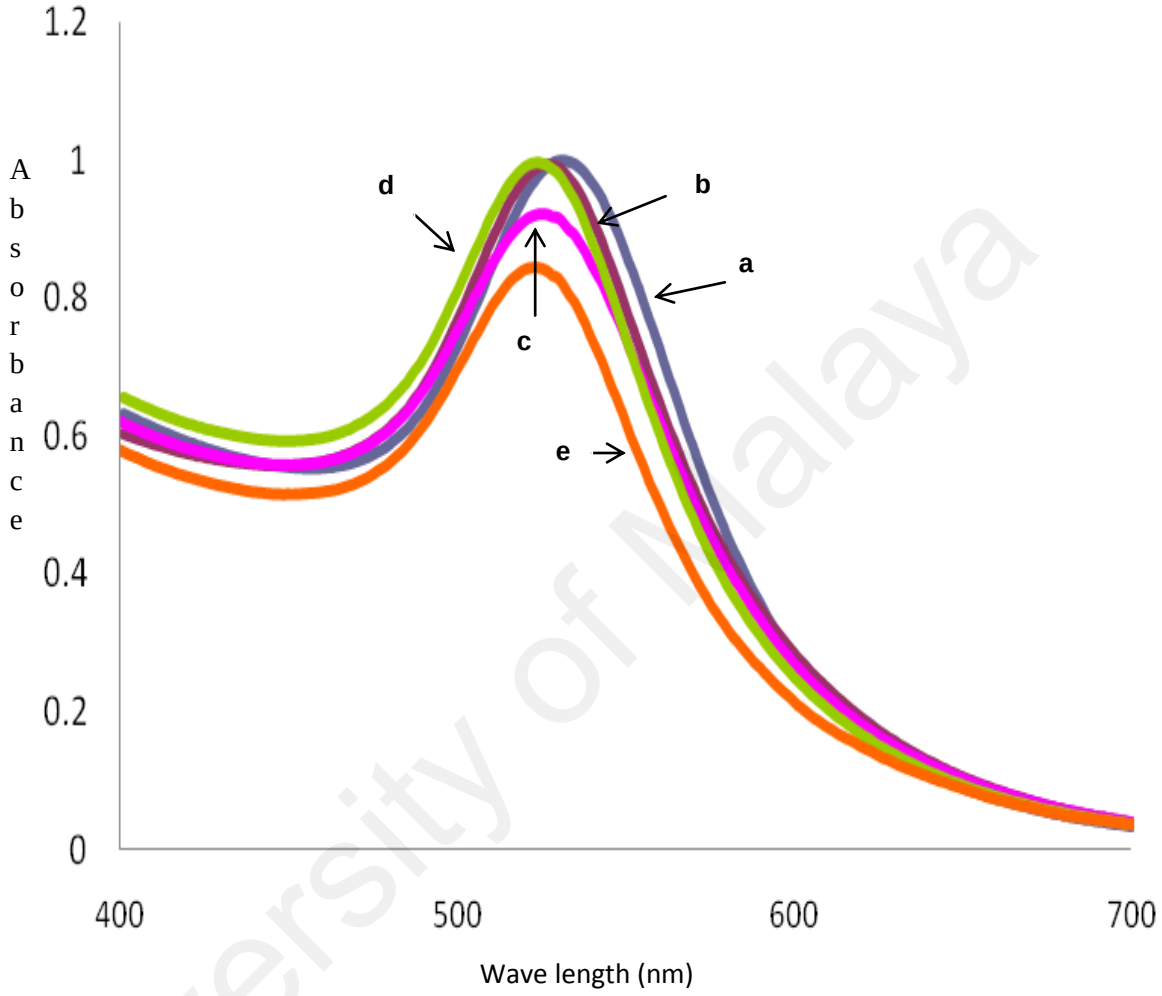

Figure 4.5: Absorption spectra of uncapped Au NPs with various concentrations of reducing agent (a:) 100 mM, (b:) 150 mM, (c:) 200 mM, (d:) 250 mM, (e:) 300 mM)

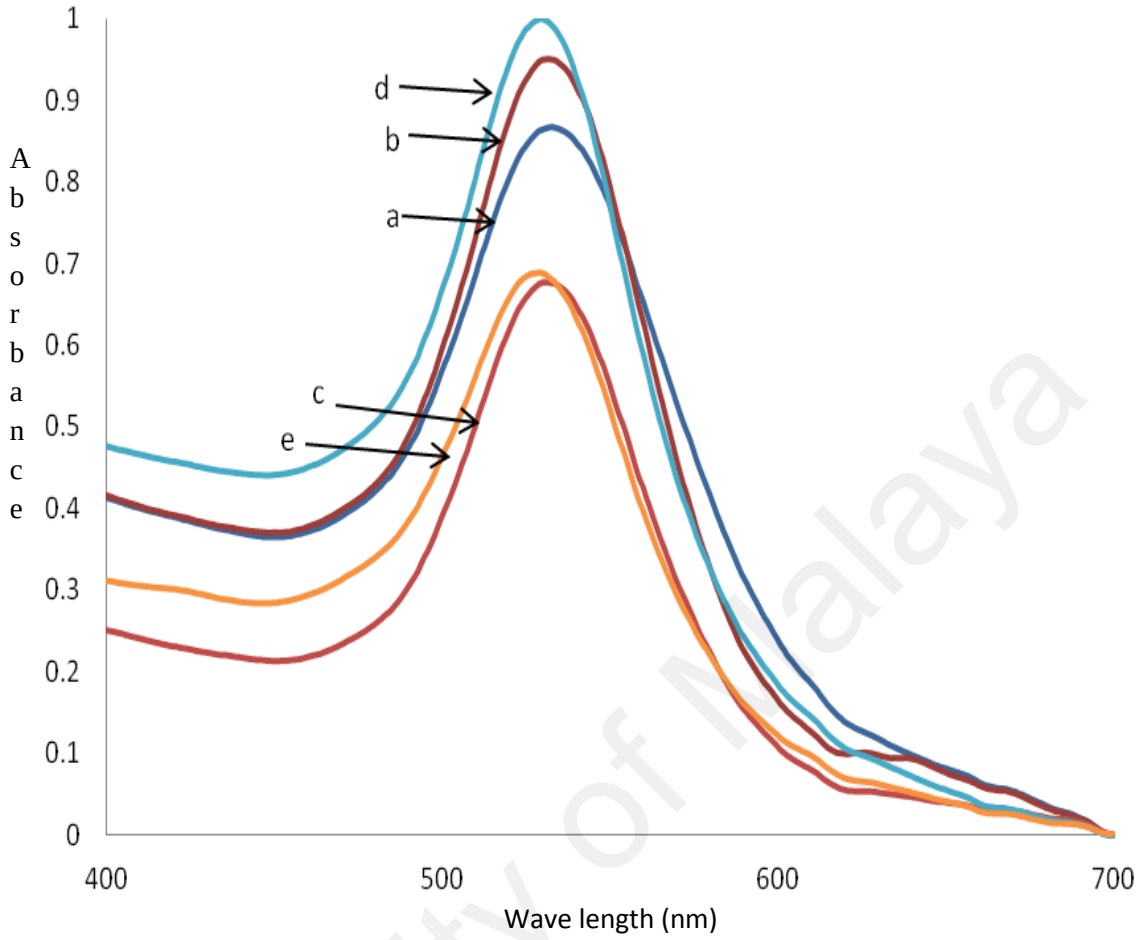

Figure. 4.6: Absorption spectra of chitosan capped Au NPs with various concentrations of reducing agent (a:)100mM, (b:) 150mM, (c:) 200mM, (d:) 250mM, (e:) 300mM, with 1 g of chitosan

Figure 4.6 shows the absorption spectra of chitosan capped Au NPs of various concentration of reducing agent for 1g of chitosan. The SPR peaks are blue shifted as the concentration of reducing agent increases. This indicates the decrease of particles sizes as the concentration of reducing agent increases. The FWHM values are also decreases indicate the narrow particles size distribution as shown in Table 4.1. This verify chitosan preserve MSG role in reducing and concurently stabilizes the gold particles.

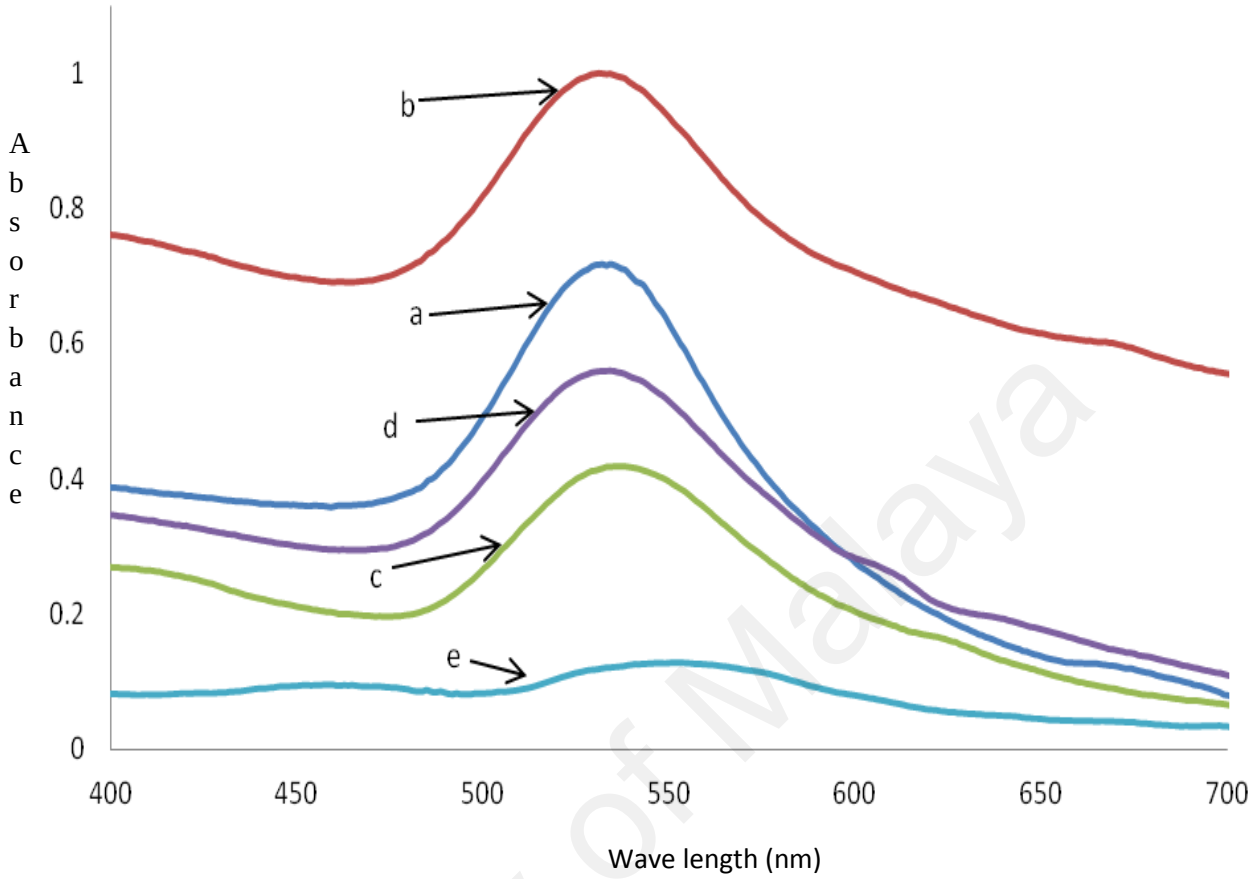

Figure. 4.7: Absorption spectra of chitosan capped Au NPs with various concentrations of reducing agent (a:) 100 mM, (b:) 150 mM, (c:) 200 mM, (d:) 250 mM, (e:) 300 mM, with 2g of chitosan

Figures 4.7-4.10 represent the absorption spectra of chitosan capped AuNPs for increased weight of chitosan. The SPR peaks for 2g of chitosan capped AuNPs has an disorder pattern as the concentration of reducing agent increases with the peaks revolves around 528 to 547 nm. The FWHM values are also with the similar pattern. This shows the instability of Au NPs with 2 g of chitosan. The FWHM values are also increases as the concentration of reducing agent increases. This shows an increase of particle size and particles size distribution. On the other hand, 3, 4 and 5 g of chitosan capped AuNPs exhibit red shifted SPR peaks as the concentration of MSG increases. Therefore, the most stable Au NPs

occurred at 1g of chitosan.

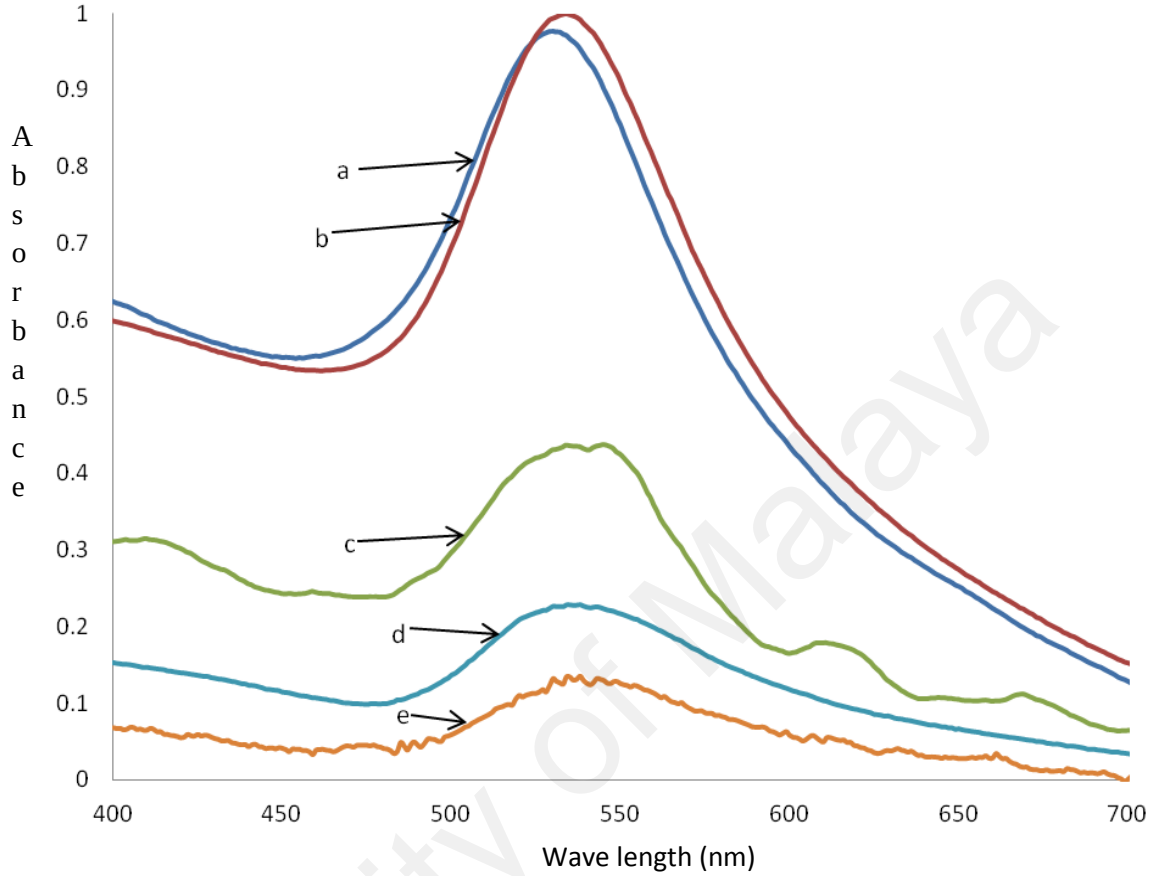

Figure 4.8 :Absorption spectra of chitosan capped Au NPs with various concentrations of reducing agent (a:) 100 mM, (b:) 150 mM, (c:) 200 mM, (d:) 250 mM, (e:) 300 mM, with 3 g of chitosan

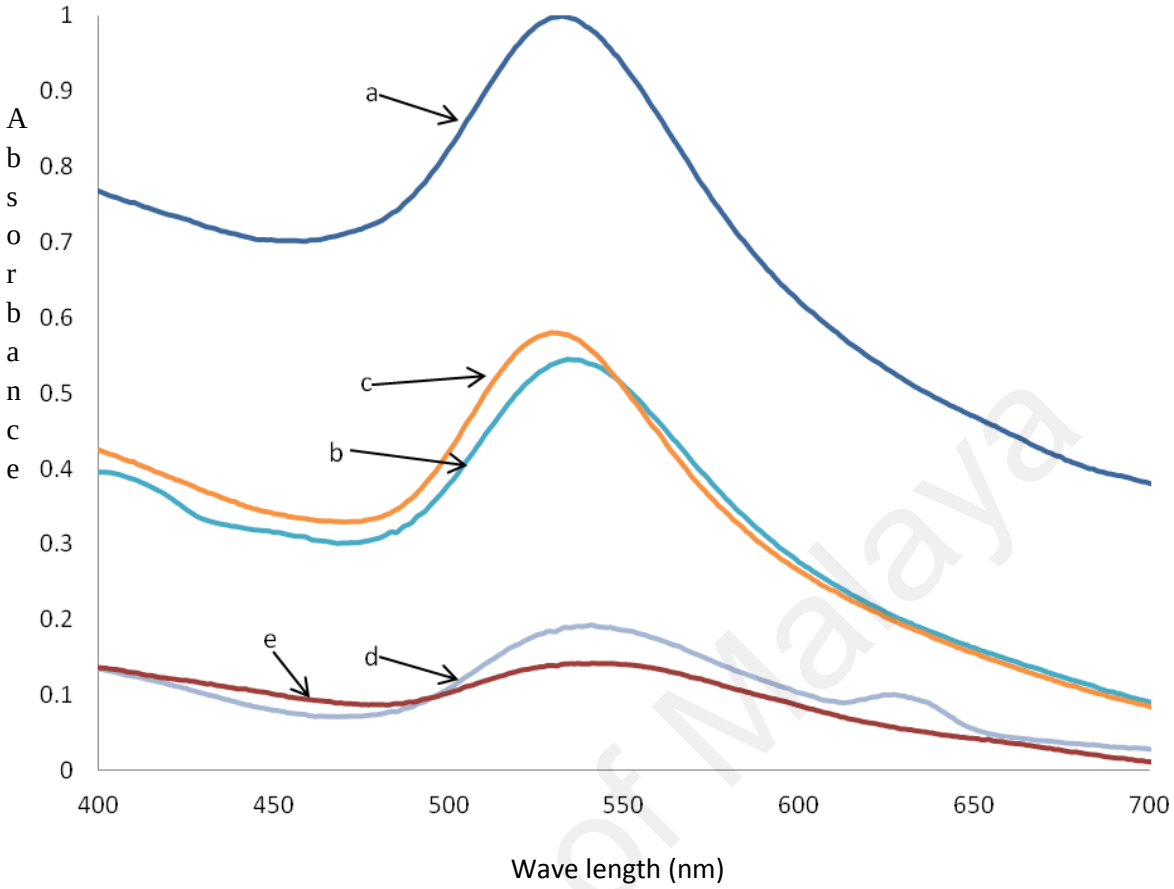

Figure 4.9 :Absorption spectra of chitosan capped Au NPs with various concentrations of reducing agent (a:) 100 mM, (b:) 150 mM, (c:) 200 mM, (d:) 250 mM, (e:) 300 mM, with 4g of chitosan

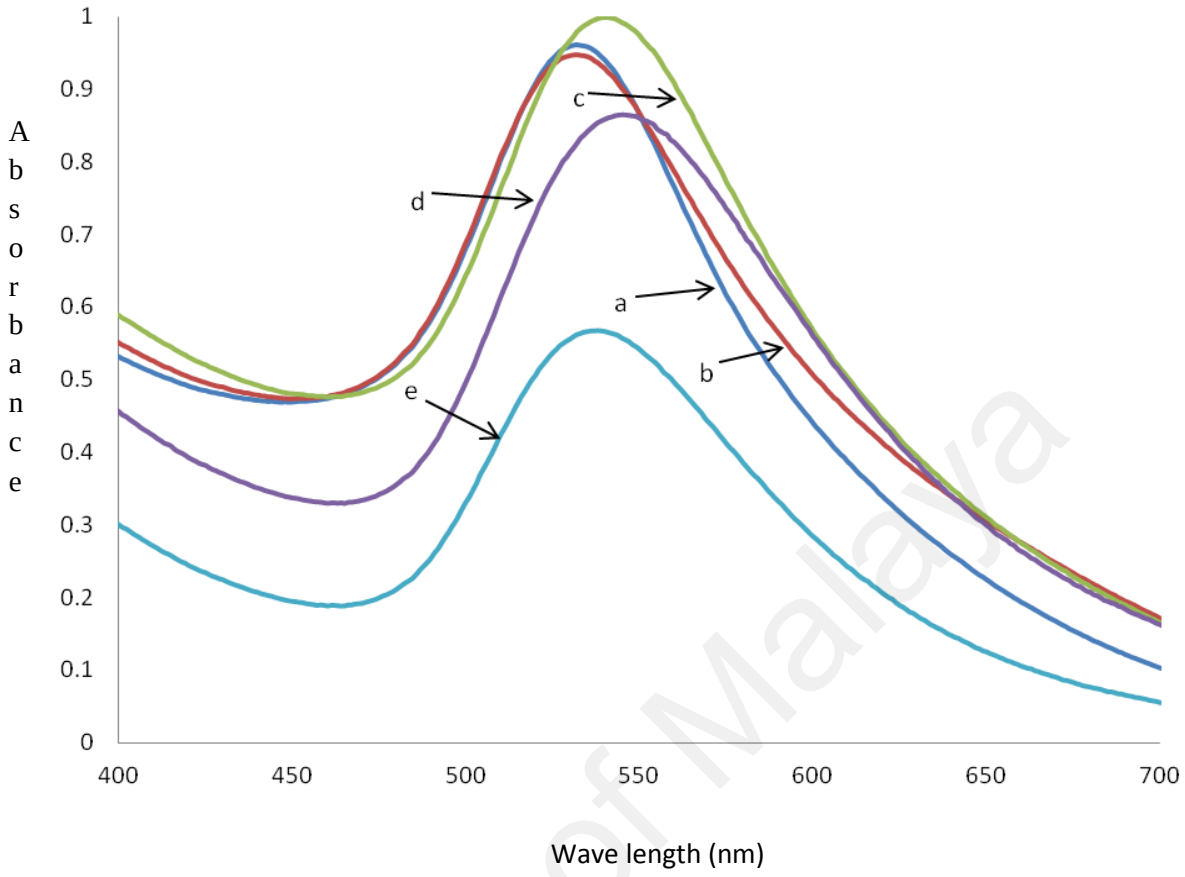

Figure 4.10: Absorption spectra of chitosan capped Au NPs with various concentrations of reducing agent (a:) 100 mM, (b:) 150 mM, (c:) 200 mM, (d:) 250 mM, (e:) 300 mM, with 5 g of chitosan

Table 4.1 summarizes the experimental values of Au NPs parametes of various concentration of MSG reducing agent.

Table 4.1: Experimental values of full width half maximum (FWHM) and surface plasmon resonance wavelength (SPR λ) for chitosan capped AuNPs reduced with various concentrations of MSG.

Sample name	MSG concentration	SPR λ (nm)	FWHM
AuNPs without capping	100 mM	532	50
	150mM	526	49
	200mM	525	52
	250mM	524	47
	300mM	523	46
AuNPs capped with 1 g of chitosan	100 mM	530	56
	150mM	528	50
	200mM	528	49
	250mM	527	46
	300mM	525	46
AuNPs capped with 2 g of chitosan	100 mM	528	53
	150mM	527	62
	200mM	533	64
	250mM	530	60
	300mM	547	62
AuNPs capped with 3 g of chitosan	100 mM	527	56
	150mM	530	53
	200mM	532	54
	250mM	533	65
	300mM	535	46
AuNPs capped with 4 g of chitosan	100 mM	528	57
	150mM	533	60
	200mM	527	51
	250mM	536	69
	300mM	538	71
AuNPs capped with 5 g of chitosan	100 mM	528	57
	150mM	528	62
	200mM	537	66
	250mM	539	65
	300mM	538	75

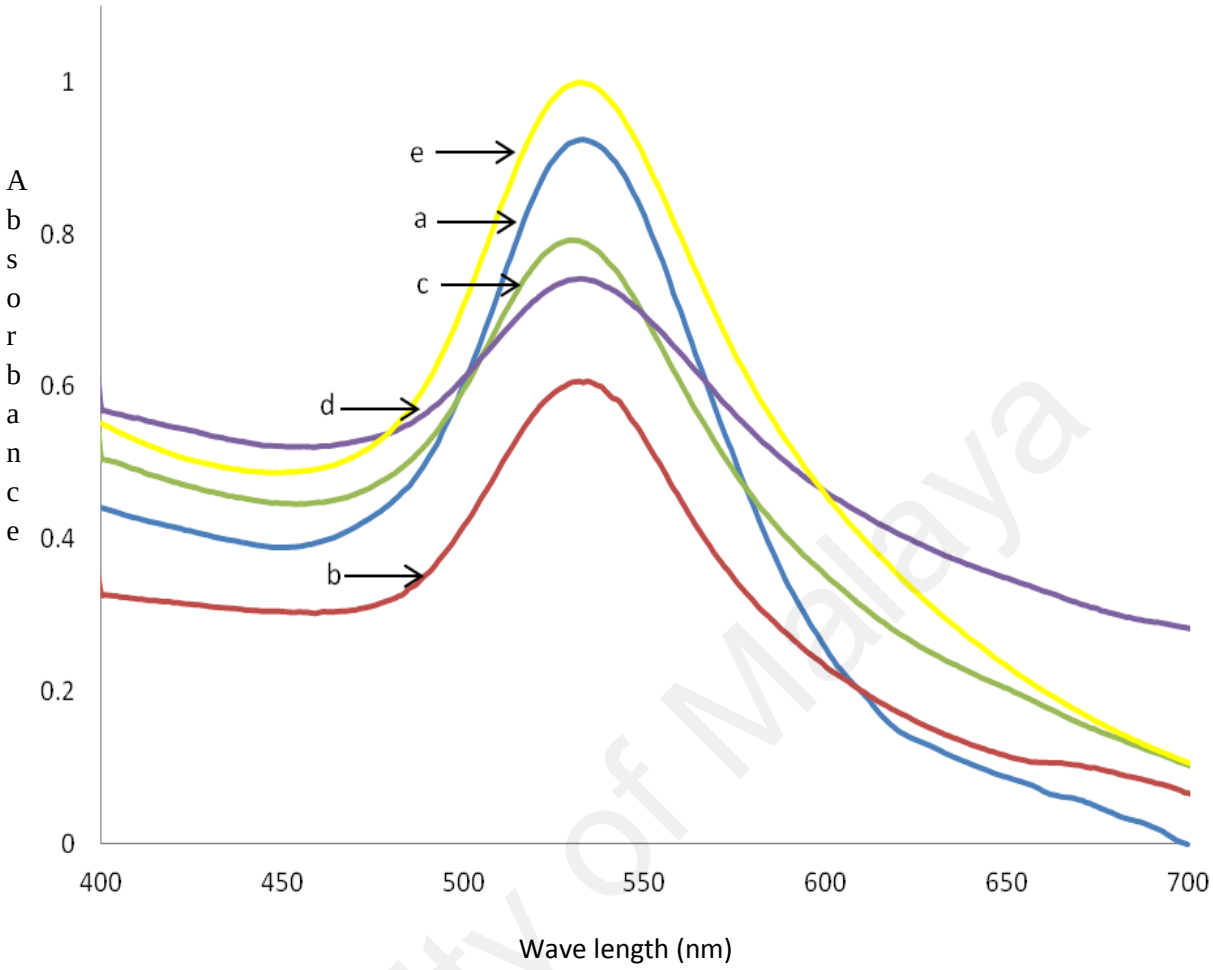

Figure. 4.11 : Absorption spectra of capped Au NPs reduced with 100 mM of MSG of various weight of chitosan (a:) 1 g, (b:) 2 g, (c:) 3 g, (d:) 4 g, (e:) 5 g

Figures 4.11-4.15 shows the absorption spectra of capped Au NPs for different concentration of reducing agent at different weight of chitosan. At lower concentration of MSG, the SPR peak and FWHM are around 528nm and 54 nm. However, as the concentration of MSG is gradually increased, the SPR peaks are slightly shifted to the larger wavelength and become broader. This indicate that the increase in particles size and particles size distribution. Table 4.2 summarizes the results.

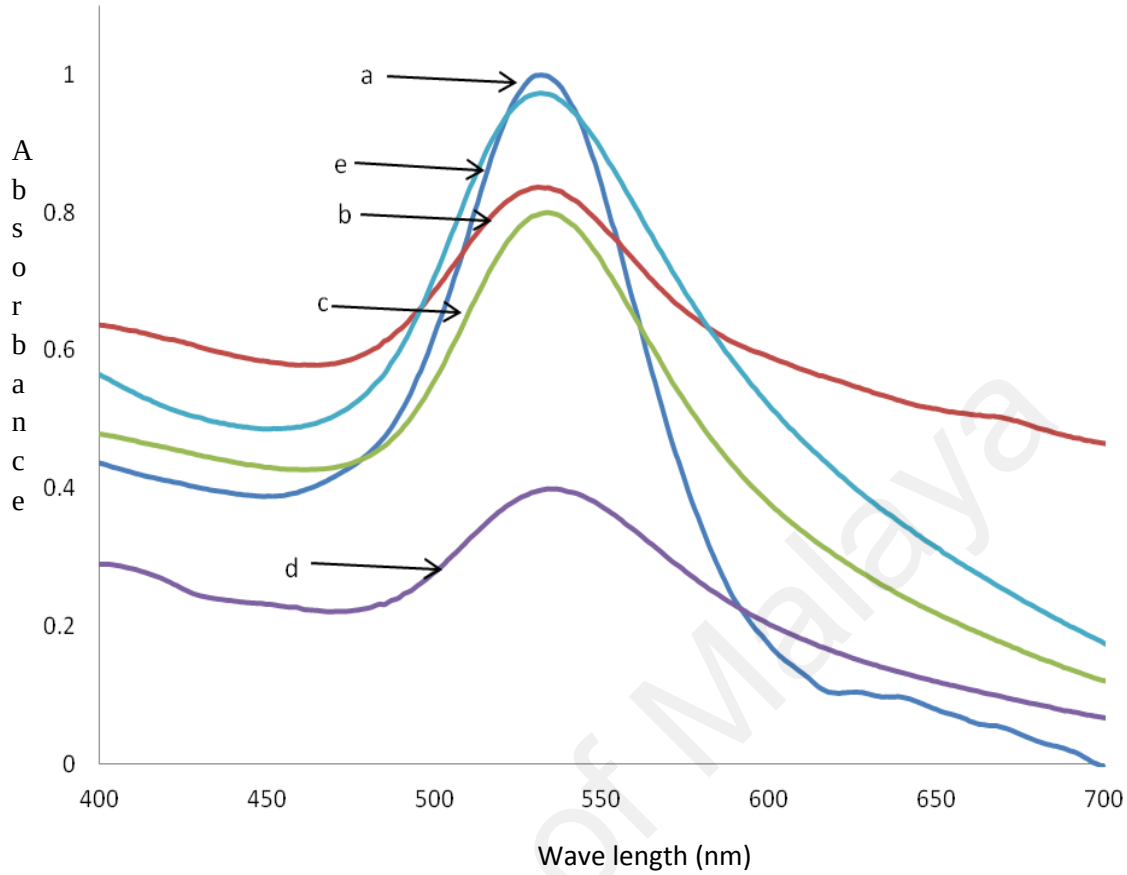

Figure 4.12: Absorption spectra of capped Au NPs reduced with 150 mM of MSG at various weight of chitosan (a:) 1 g, (b:) 2 g, (c:) 3 g, (d:) 4 g, (e:) 5 g.

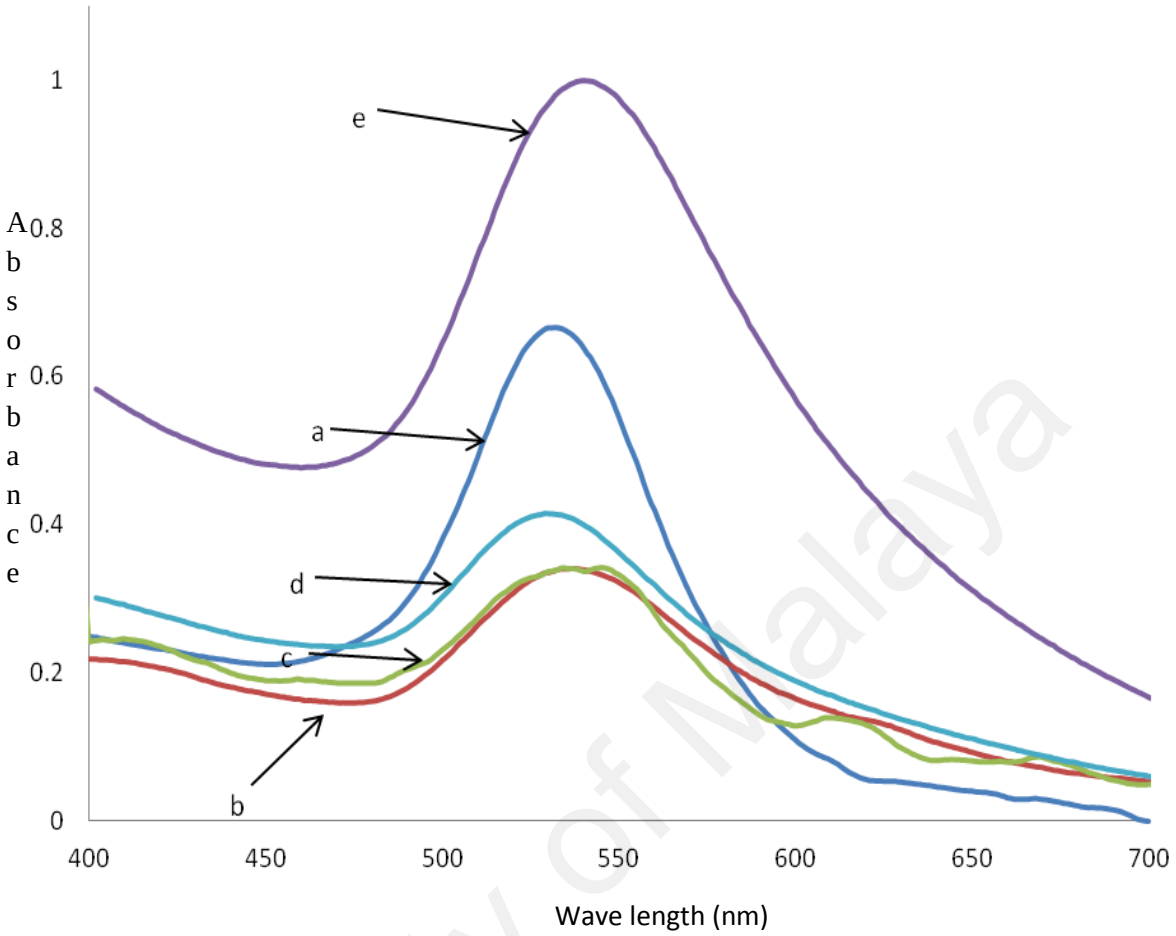

Figure 4.13: Absorption spectra of capped Au NPs reduced with 200 mM of MSG at various weight of chitosan (a:) 1 g, (b:) 2 g, (c:) 3 g, (d:) 4 g, (e:) 5 g.

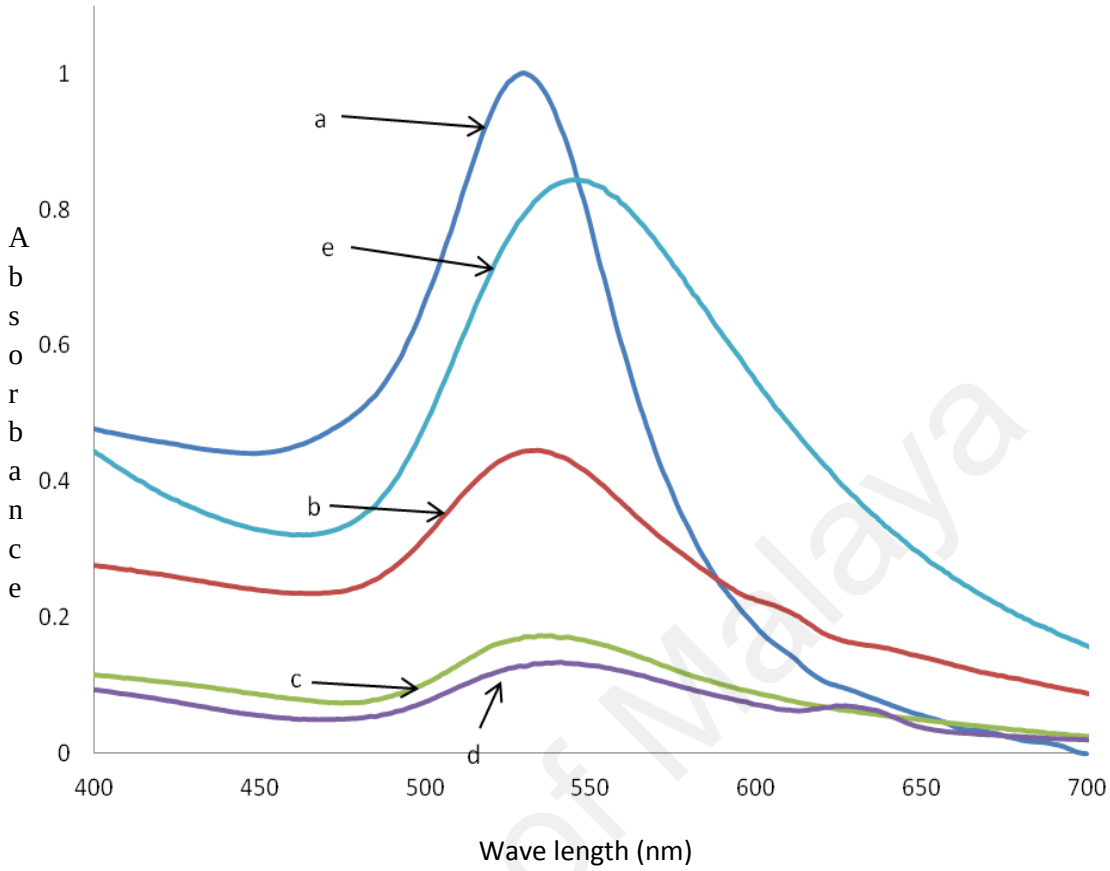

Figure 4.14: Absorption spectra of capped Au NPs reduced with 250 mM of MSG at various weight of chitosan (a:) 1 g, (b:) 2g, (c:) 3g, (d:) 4g, (e:) 5g.

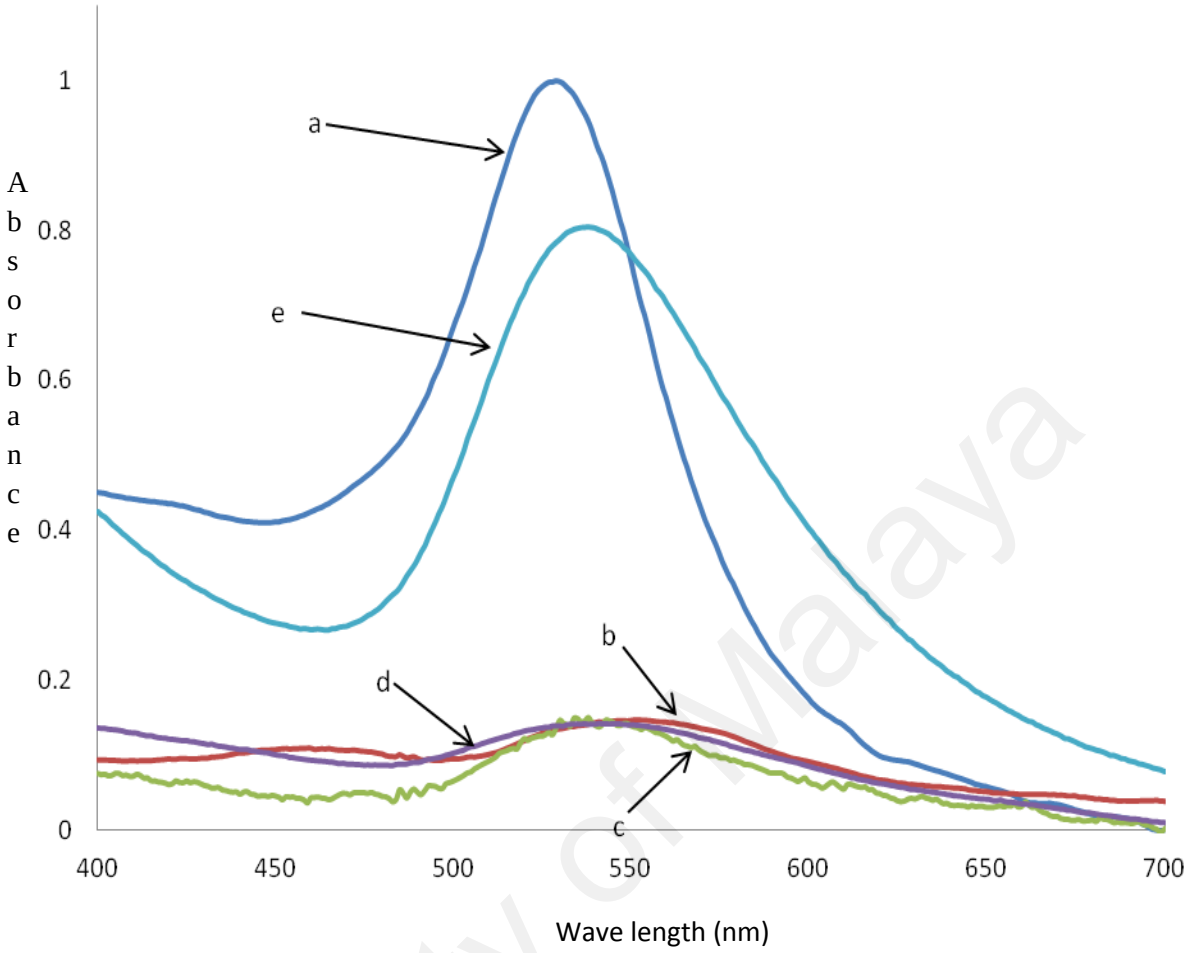

Figure 4.15: Absorption spectra of capped Au NPs reduced with 300mM of MSG at various weight of chitosan (a:) 1 g, (b:) 2 g, (c:) 3 g, (d:) 4 g, (e:) 5 g.

Table 4.2: Experimental data of full width half maximum (FWHM), SPR peak for Au NPs reduced at different concentration of MSG and various weight of chitosan

Concentration of MSG (mM)	Weight of Chitosan (g)	SPR peak (nm)	FWHM
100	1	530	56
	2	528	53
	3	527	56
	4	528	57
	5	528	57
150	1	528	50
	2	527	62
	3	530	53
	4	533	60
	5	528	62
200	1	528	46
	2	533	64
	3	532	54
	4	527	51
	5	537	66
250	1	527	46
	2	530	60
	3	533	54
	4	536	69
	5	539	65
300	1	525	46
	2	547	62
	3	535	46
	4	538	71
	5	538	75

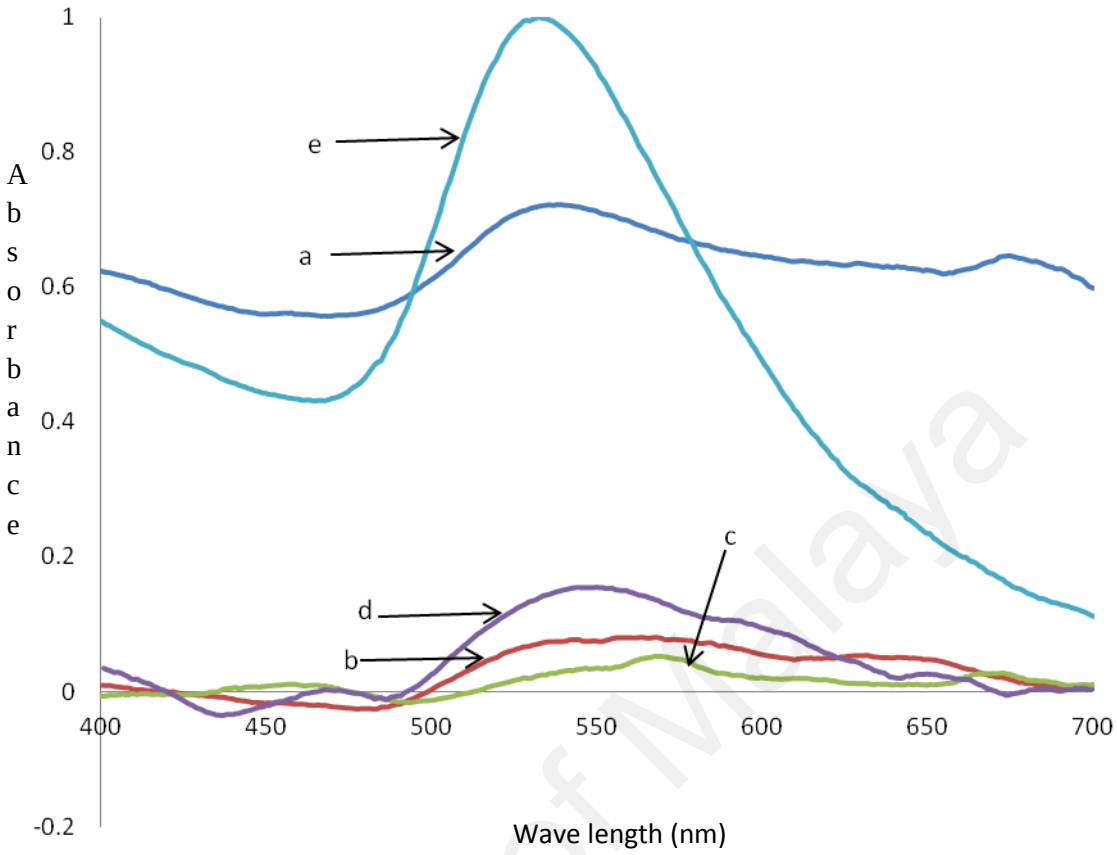

Figure 4.16: Absorption spectra of uncapped Au NPs reduced with various concentration of MSG after 1 month aging time (a:) 100 mM, (b:) 150 mM, (c:) 200 mM, (d:) 250 mM, (e:) 300 mM

Figure 4.16 shows the uncapped Au NPs with various concentration of MSG after 1 month aging time. The SPR peaks are of Au NPs after 1 month aging time are occurred at longer wavelength compared to their counterparts in Figure 4.4. The case is also true for the FWHM values after 1 month aging time which show increase in broadening. This indicates that the size of particles and particle size distribution are increased after aging.

Table 4.3 Experimental values of full width half maximum (FWHM) and SPR peak for Au NPs after 1 month aging time.

Concentration Reducing Agent (mM)	SPR λ_{max}(nm)	SPR λ_{max}(nm) after 1 month	FHWM(nm)	FHWM(nm) after 1 month
100	532	532	50	51
150	526	544	49	72
200	525	554	52	52
250	524	544	47	96
300	523	534	46	70

Figure 4.17 shows the absorption spectra of capped Au NPs for various concentration of MSG after aging 1 month. The SPR peaks occurred at smaller wavelength compound to the uncapped Au NPs (Figure 4.16). Their FWHM values are smaller compounds the uncapped Au NPs. This absorption spectra have highlighted the role of chitosan adsoprtion on the gold particles surfaces, in which gold particles stay small even after 1 month. The gold particles in the solution preserves stability and hinder agglomeration. The chitosan capped Au NPs are more intensed even after 1 month compared to non capped Au NPs. The FWHM and other experimental results are listed in Table 4.4.

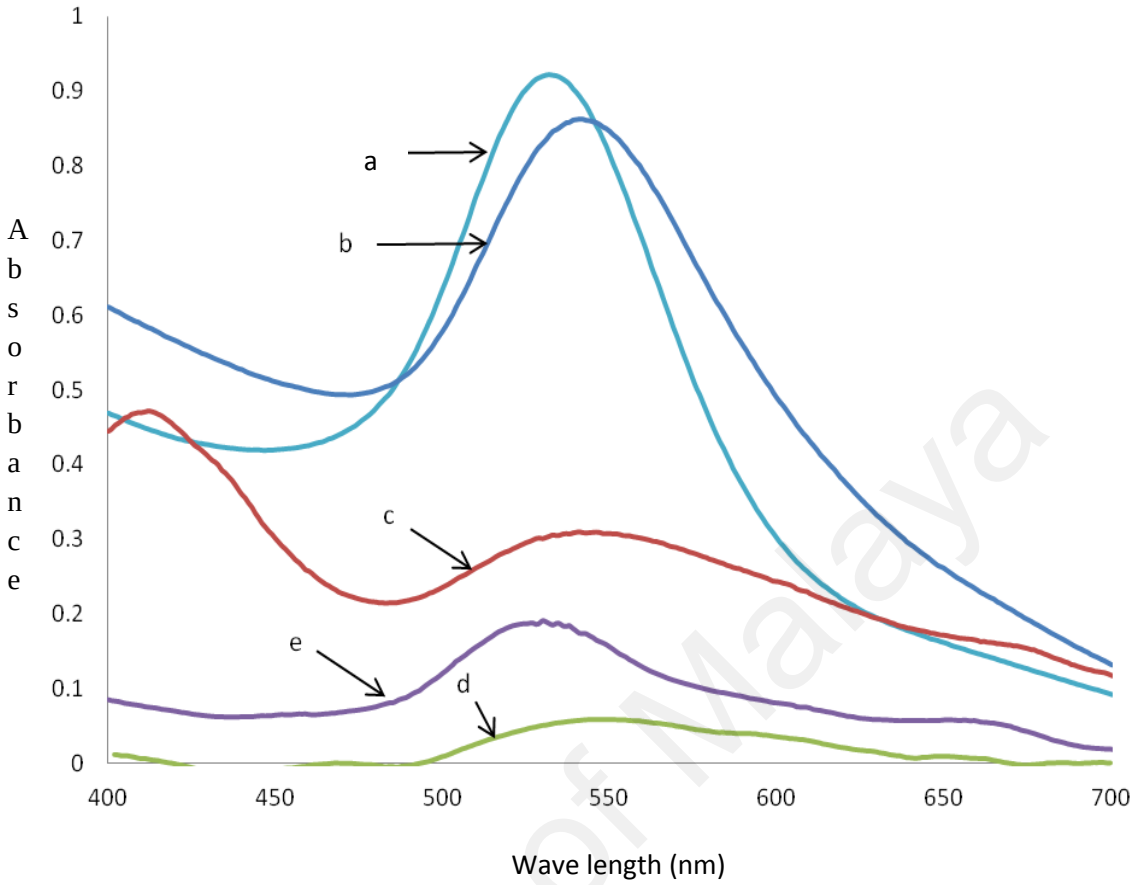

Figure 4.17: Absorption spectra of capped Au NPs reduced with various concentration of MSG after 1 month aging time (a:) 100 mM, (b:) 150 mM, (c:) 200 mM, (d:) 250 mM, (e:) 300 mM

Table 4.4 Experimental values of full width half maximum (FWHM) for chitosan capped AuNPs after 1 month

Concentration of MSG (mM)	SPR λ_{max}(nm)	SPR λ_{max}(nm) after 1 month	FHWM(nm)	FHWM(nm) after 1 month
100	530	531	56	60
150	528	537	50	52
200	52	539	49	51
250	527	527	46	46
300	525	526	46	57

The behaviour of Au NPs at various holding time is shown in Figure 4.18. The Au NPs were reduced by 50 mM of MSG and the period of holding time was recorded right after the addition of MSG. A gradual increase of peak intensity can be observed notifying the progress of the reduction and stabilization process towards development of size reduced-Au NPs. Samples with higher relaxation time were able to disrupt the attempt of the metallic gold from growing onto Au NPs. Broad absorbance spectra can be observed at the shortest holding time with FWHM of 125 (Table 4.5) and subsequently yield to sharper peaks at maximum holding time with FWHM of 52.

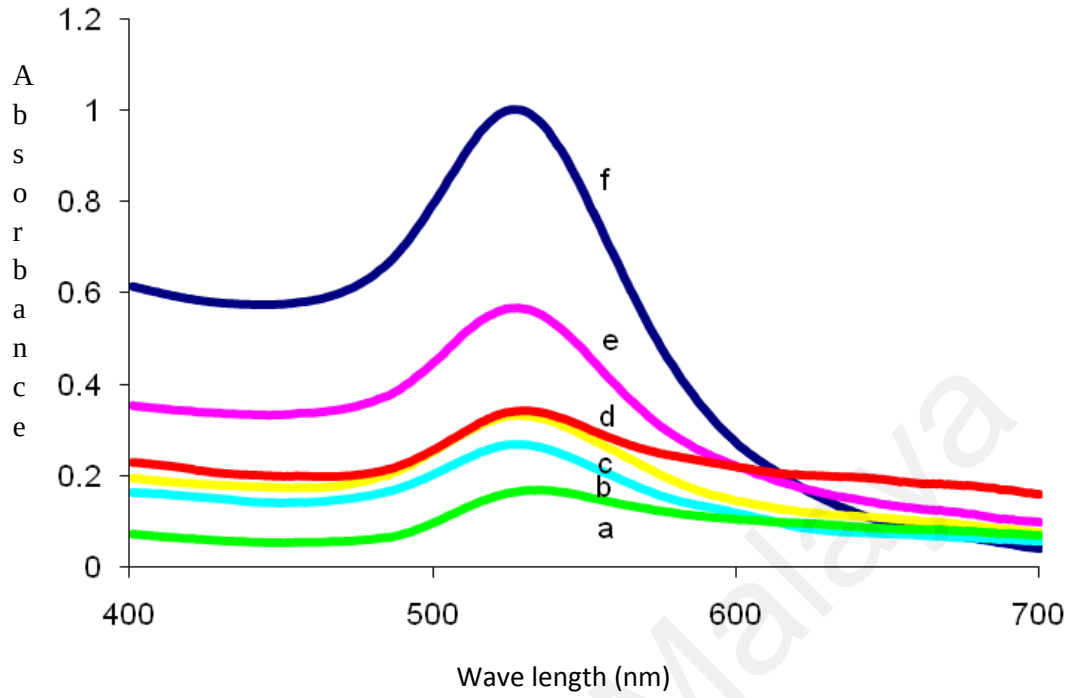

Figure 4.18: Absorption spectra of Au NPs at various holding time (a:) 10 min, (b:) 15 min, (c:) 20 min, (d:) 25 min, (e:) 30 min, (f:) 35 min

Table 4.5 Experimental values of full width half maximum (FWHM) and SPR peaks for Au NPs.

Time (min)	SPR (nm)	FWHM(nm)
10	531	125
15	523	59
20	523	59
25	526	55
30	521	52
35	521	52

4.3 Theoretical study of chitosan capped Au NPs

Figure 4.19 shows the absorption spectra of capped Au NPs for various chitosan to $AuCl_3$ concentration ratio. At lower concentration ratio, the SPR peaks occurred at larger wavelength. As chitosan concentration increases, the SPR peaks slightly shifted to smaller wavelength.

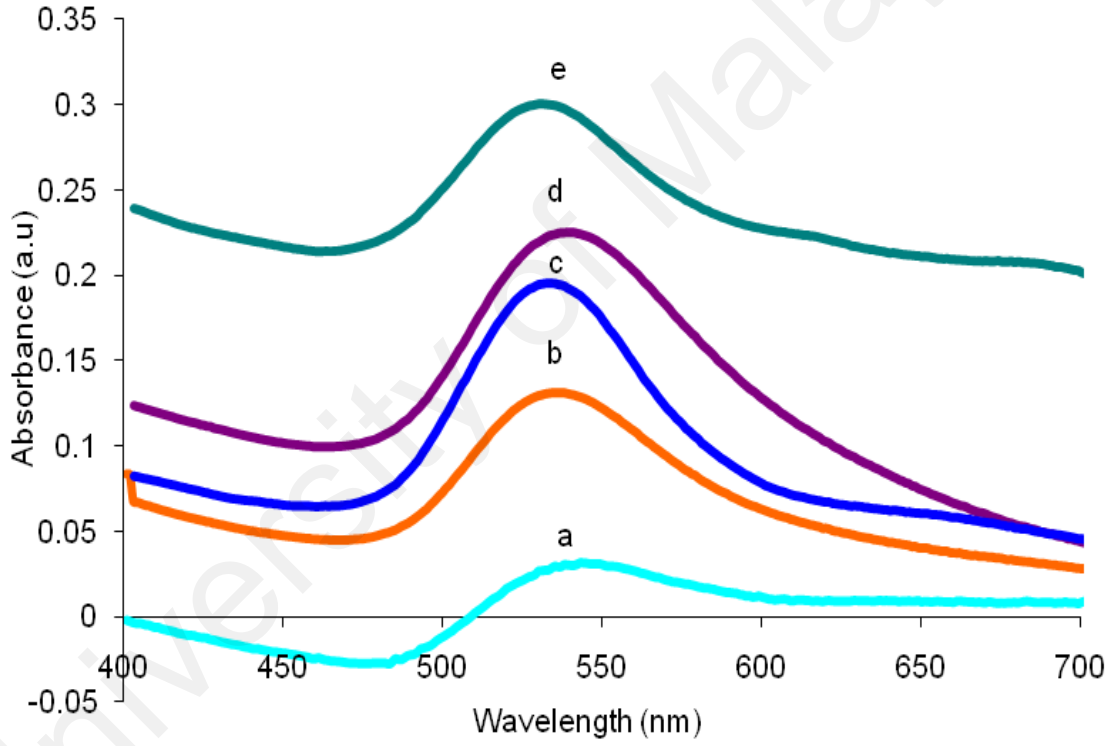

Figure 4.19: Absorption spectra of chitosan capped Au NPs at various chitosan to $AuCl_3$ concentration ratio (a:)0:1, (b:)1:1, (c:)1.5:1 , (d:)2:1, (e:) 2.5:1

Figure 4.20 was plotted from the equation below:

$$\frac{1}{\Delta A} \approx \frac{1}{K_{eq}\ d}\left(\frac{1}{[chitosan]}\right) + \frac{1}{d} \qquad (4.1)$$

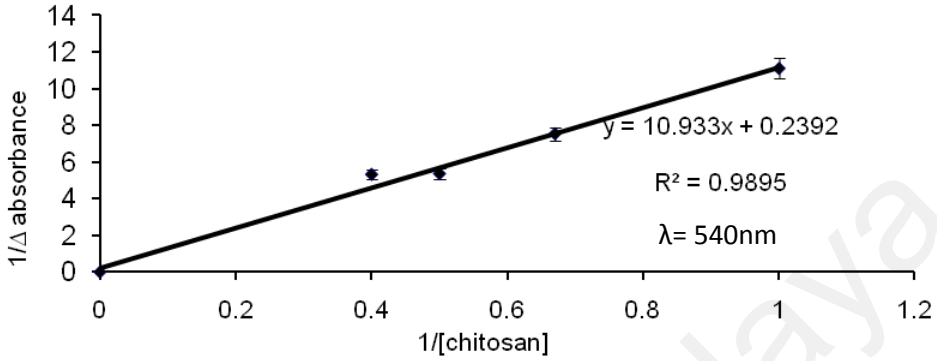

Figure 4.20: Graph of $\frac{1}{\Delta Absorbance}$ versus $\frac{1}{[chitosan]}$ for chitosan-labeled Au NPs

where d = $[Au\ NPs]\,\varepsilon_c\,\ell$, ΔA is the delta absorbance of two absorption spectra logged at corresponding wevelength, K_{eq} and ε_c is the equilibrium constant and extinction coefficients of the new complex respectively. While ℓ is optical wavelength which is equal to 1 cm.

By fitting the data, the slope and intercept from the graph $\frac{1}{\Delta A}$ versus $\frac{1}{([chitosan])}$ graph are $\frac{1}{K_{eq}[Au\ NPs]\,\varepsilon_c\,\ell}$ and $\frac{1}{[Au\ NPs]\,\varepsilon_c\,\ell}$. The Gibbs free energy can be obtained using equation below:

$$K_{eq} = e^{\frac{-\Delta G}{RT}} \qquad (4.2)$$

where K_{eq}= equilibrium constant, ΔG = Gibbs free energy, R= gas constant and T= ambient temperature. By varying the chitosan concentration of chitosan capped Au NPs, the

absorption spectra (Figure 4.19) generates the plot of the graph of 1/ Δ absorbance versus 1/ [chitosan] (Figure 4.20). The delta absorbance was logged at 540 nm wavelength and the concentration of reducing agent was 50 mM. The value of K_{eq} and ΔG of Au NPs reduced with 50 mM of MSG capped with chitosan were computed as 0.0219 mol L^{-1} and -12.22 kJ mol^{-1}. As a comparison, the value of ΔG for Au NPs adsorbed by bovine serum albumin (BSA) was -1196.8 kJ mol^{-1} (Maleki et al., 2012). The value of ΔG was negative to corroborate the reaction was spontaneous and stable from thermodynamic point of view (Wade, 2006). A smaller value of ΔG of a chemical reaction is desirable owing to greater driving force of adsorption and small adsorption capacity. A small adsorption capacity was credited to extension of adsorption surface (Wang & Zhu, 2007). In this section, it was concluded that chitosan was attested to be more stable and adsorbed surface of Au NPs efficiently.

4.4 Effect of amorphous-carbon nanotube (α-CNTs)s, oxides and sulphate to chitosan capped Au NPs

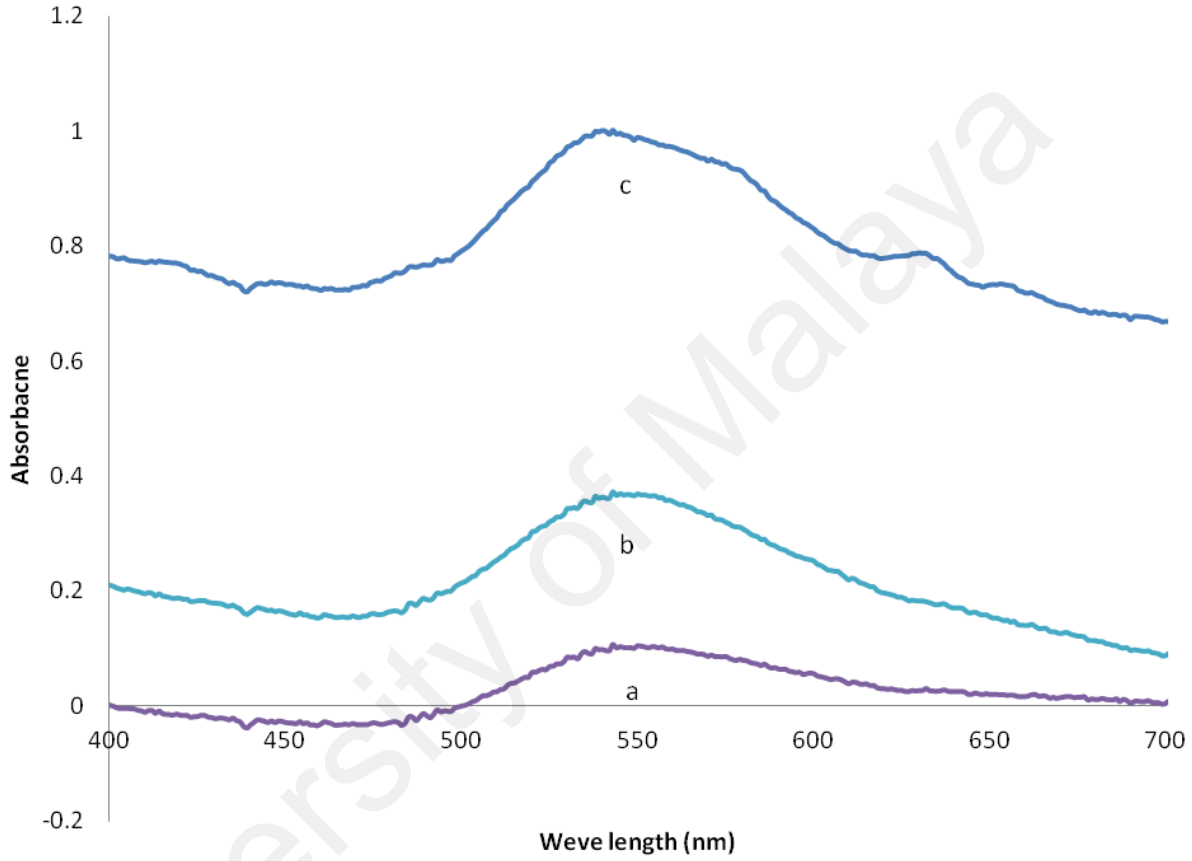

Figure. 4.21:Absorption spectra of amorphous carbon nanotubes (α-CNTs) -chitosan capped Au NPs at various carbon nanotubes weight (a:) 0.001 g, (b:) 0.005 g, (c:) 0.05 g

Figure 4.21 shows the SPR peak position adjourned at wavelength of 549 nm for three different weight of carbon nanotubes. On the contrary, the peak intensity rises as the carbon nanotubes weight were increased. The spectra in Figure 4.21 (a) has highlighted the red shifting of SPR peaks if compared to spectra in Figure 4.1 (a) which represent chitosan capped Au NPs. The peak shifting corresponded to capturing of carbon nanotubes by chitosan Au NPs. The free amines in chitosan structure have attest its ability to uptake

analyte, carbon nanotubes as emphasized.

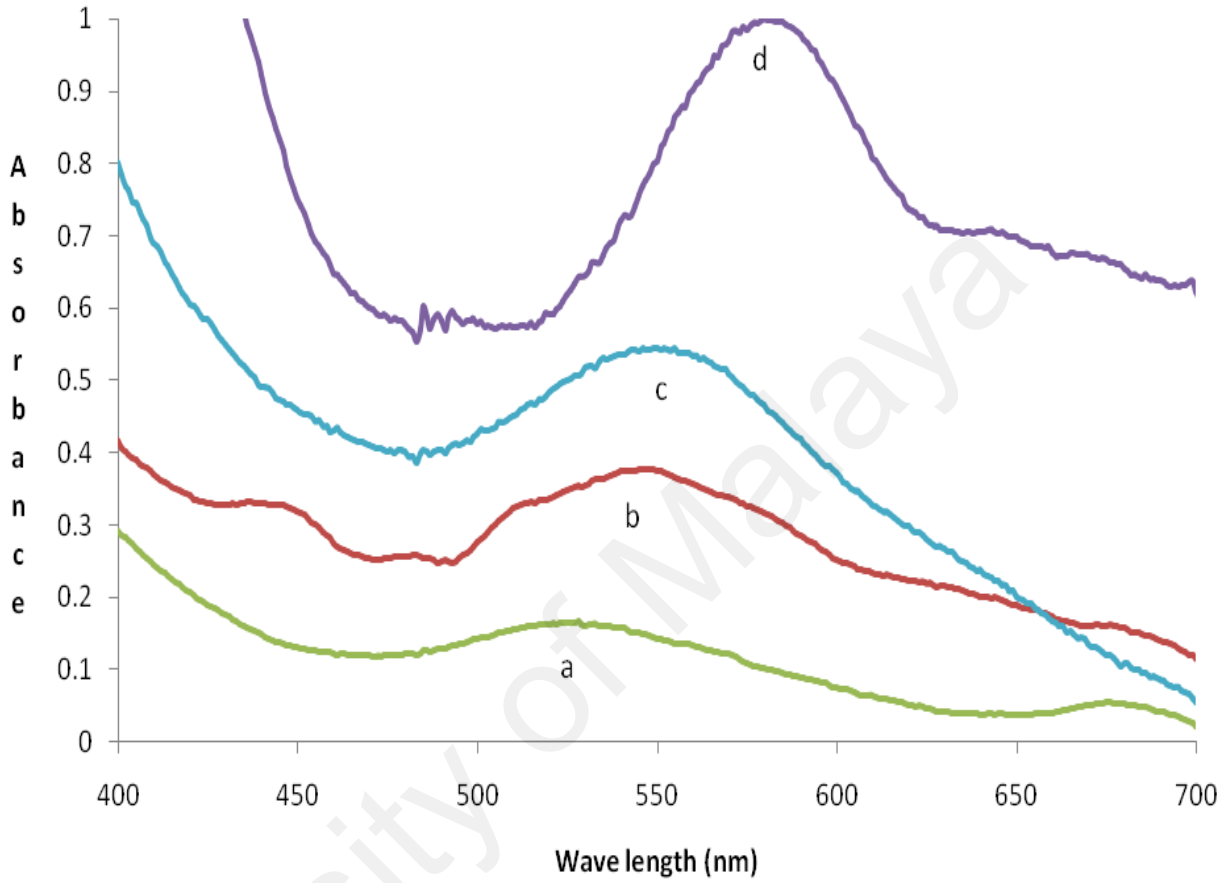

Figure. 4.22:Absorption spectra of copper oxide-chitosan capped Au NPs at various copper oxide weight (a:) 0.005 g, (b:) 0.01 g, (c:) 0.05 g, (d:) 0.1 g

Figure 4.22 shows the absorption spectra of copper oxide- chitosan capped Au NPs at for 0.005 g, 0.01 g, 0.05 g, and 0.1 g. The SPR peaks have shifted from 521 nm to 577 nm as the weight of copper oxide increases up to 0.1 g. This clearly shows the combination of chitosan capped Au NPs towards addition of copper oxide to the solution. The enlargement of the particles uptake can be underlined as the peak intensity also shows dramatic increased as the weight of copper oxide increases. Figure 4.22 is identical to Figure 4.21 where red shifting of the SPR peaks compared to spectra in Figure 4.1 (a) was attested.

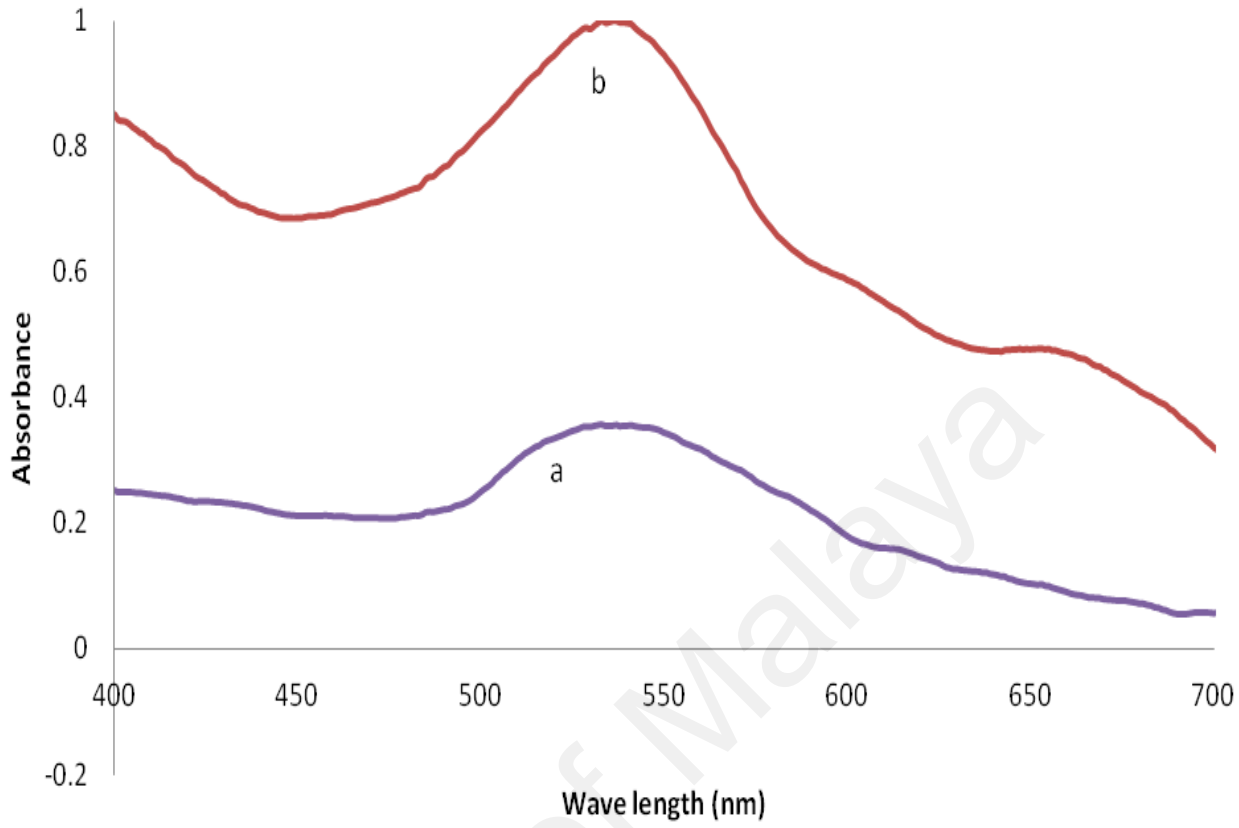

Figure. 4.23:Absorption spectra of zinc sulphate-chitosan capped Au NPs at various zinc sulphate weight (a:) 0.01 g, (b:) 0.05 g

Figure 4.23 shows the absorption spectra of zinc sulphate- chitosan capped Au NPs at for 0.01 g and 0.05 g. As discussed in previous spectra, this spectra also successfully shows analyte particles entrapment by chitosan capped Au NPs. The SPR peaks are sharper as the weight of zinc sulphate added to the chitosan capped Au NPs solution. The peaks also shifted to the right as the weight of zinc sulphate increases to 0.05 g. The findings in above absorption spectra with three different target material has underlined the suitability of Au NPs as a chemical sensor.

Chapter Five

CONCLUSION AND FUTURE RECOMMENDATIONS

CHAPTER FIVE

Conclusion

5.1 Conclusion

The synthesis and characterization of Au NPs and chitosan capped Au NPs has been investigated. The main focus of this research had been achieved in which the in depth analysis of Au NPs and chitosan Au NPs were carried out. The correlation of concentration of reducing agent and stabilizer to the properties of Au NPs and chitosan capped Au NPs had been presented efficiently. The utilization of stabilizer to Au NPs potentially for the use as chemical sensor had been performed thoroughly.

At high concentration of MSG as reducing agent, the surface plasmon absorption peak was recorded to be in the range of 523-532 nm for uncapped Au NPs. The proportionality of size of gold particles and concentration of MSG were recorded as inversed. The absorption spectra were blue shifted and the FWHM declines as the concentration of MSG reaches 300 mM. On the other hand, the absorption intensity was observed to be constant and start to

decline at the 300mM of MSG. These comprehend to be the high excess of Na^+ ions from MSG which create gloominess within the particles.

It is observed holding time significantly affect the particles size of uncapped Au NPs. The absorption spectra shows gradual increased in absorption intensity and decreased in FWHM as holding time increases. The pattern indicates the smaller particles size and narrow size distribution for longer holding time.

Chitosan has been observed to resembles spider web and obstruct agglomeration between gold particles. Hence, the Au NPs are been isolated between each other and well dispersed. The absorption spectra of chitosan capped Au NPs had showed departure which signify changes in dielectric constant of the solution.

The chitosan capped Au NPs has showed blue shifted surface plasmon absorption peak for 1 g of chitosan with increased concentration of MSG. The SPR peaks were recorded to be in the range of 525-530 nm. The FWHM has also declined as the concentration of MSG increases. The results were matched up to the uncapped Au NPs ones and point up that chitosan preserved role of MSG in gold particles reduction and simultaneously stabilizes the particles. On the contrary, red shifting of surface plasmon resonance peak was recorded for 2, 3, 4 and 5 g of chitosan capped Au NPs. The disorder pattern were unliked 1 g of chitosan and highlighted 1 g of chitosan to be the optimum weight of chitosan as stabilizer in this case.

The aging time has shows the ability of chitosan to preserves particles size and stability of

Au NPs. From the Uv-Vis absorption spectra, blue shifting has been observed between SPR peaks for the chitosan capped Au NPs aged for 1 month followed by decreased in FWHM as the concentration of MSG increases. However, the particles size agglomerated and enlarged due to absence of stabilizer for uncapped Au NPs aged for 1 month. The absorption spectra has encountered red shifting between the SPR peaks of uncapped Au NPs and increased in FWHM as the concentration of MSG increases.

The thermodynamic stability was studied though an extended method of Benesi Hildebrand. The Gibbs free energy of Au NPs reduced with 50 mM of MSG was calculated to be -12.22 kJ mol^{-1}. The studies were commenced thru an absorption spectra of different concentration of chitosan capped Au NPs logged at 540 nm. Then, it was furthered by plotted of graph 1/ Δ absorbance versus 1/ [chitosan]. The Gibbs free energy value was obtained by deliberating the slope and intercept of the graph.

The effieciency of chitosan capped Au NPs uptaking target materials were successfully examined with amorphous carbon nanotubes (α-CNTs), copper (II) oxide (Cu_2O) and zinc sulphate ($Zn\ SO_4$). The absorption spectra of these three target material with chitosan capped Au NPs has underlined the gradual increased in absorption intensity and peak shifting to the longer wavelength. The suitability of Au NPs as a chemical sensor has been clearly highlighted.

As a conclusion, Au NPs with enhanced properties has been achieved by altering the process parameters. The Au NPs are stable, homogenous and apt for chemical sensing purposes after capped with chitosan.

REFERENCES

References:

Antonii, F., Panacea Aurea-Auro Potabile, Bibliopolio Frobeniano, Hamburg, 1618.

Bendayan, M., J. Histochem. Cytochem., **29**, 531-541 (1981).

Blaber, M., (2002) Chemical Thermodynamics: Gibbs Free Energy. http://www.mikeblaber.org/oldwine/chm1046/notes/Thermody/Gibbs/Gibbs.htm. Accessed May 26, 2010

Brust, M.,Walker, M., Bethell, D., Schiffrin, D.J.,Whyman, R., Chem. Commun., **7**, 801 (1994).

Buffat, P.H., Borel , J.P., Phys. Rev. A, **13**, 2287–2298 (1976).

Cao, L., Diao, P., Tong, L., Zhu, L., Liu, Z., Chem. Phys. Chem., **6**, 913-918 (2005).

Cheng, S.F., Chau, L.K., Anal. Chem .,**75**, 16-21 (2003).

Crooks, R.M., Lemon, B.I., Yeung, L.K., Zhao, M.Q., Top. Curr. Chem., **212**, 81-135 (2000).

Daniel, M.C., Astruc, D., Chem Rev, **104**, 296-298 (2004).

Dawson, A., Prashant, V.K., J. Phys. Chem. B, **104** (50), 1184211846 (2000)

Durr, N.J., Larson, T., Smith, D.K., Nano Lett, **7**, 9415 (2007).

Dutta, J., Sugunan, A., Thanachayanont, C., Hilborn, J.G., Sci and Tech of Adv Mater, **6**, 335-340 (2005).

Faraday, M., Philos. Trans.,**147**, 145-181 (1857).

Frederix, F., Friedt, J., Choi, K., Laureyn, W., Campitelli, A., Mondelaers, D., Maes, G., Borghs, G., Anal. Chem. **75**, 6894-6900 (2003).

Freeman, R., Hommer, M., Grabar, K., Jackson, K., Natan, M., J. Phys. Chem., **100**,718-724 (1996).

Frens, G., Colloid Polymer Science, **250**, 736-741 (1972).

Fu, Y., Qiu, M., Optical Properties of Nano Structures, Pan Stanford publishing Pte Ltd. Singapore, 268 , 2011.

Fujiwara, K., Watarai, H., Itoh, H., Nakahama, E., Ogawal, N., Anal. Bioanal. Chem., **386**, 639-644 (2006).

Gasparyan, V.K., Current clinical pharmacology,**4** (2), 159-163 (2009).

Guibal, E., Separation and Purification Technology, 38, 43-74 (2004).

Hamaker, H.C., Physica, **4**(10), -10581072 (1937).

Handley, D.A., in: Hayat, M.A., (Ed.) Colloidal Gold: Principles, Methods, and Applications, Academic Press, New York. 1 (1989).

Herrera, A.P., Oscar, R., Julio, G.B, Carlos, R., Nanotechnology, **16**, 618 (2005)

Hoffman, J., Zin, M., He, Y., (2006), Nanotechnology in biomedicine, http://courses.washington.edu/overney/ChemE554_Course_Mat/Biomedicine.doc. Accessed on May 26, 2010

Hone, D.C., Haines, A.H., Russell, D.A., Langmuir, **19**, 7141–7144 (2003).

Hosokawa, M., Nogi,K., Naito, M., Yokoyama, T., (Eds.). Nanoparticles Technology Handbook, Elsevier ,Netherlands, 2007.

Huang, C.C., Huang, Y.F., Cao, Z., Tan, W., Chang, H.T., Anal. Chem., **77**, 5735–5741 (2005).

Huang, X., El-Sayed, M.A., Journal of Advanced Research, **1**, 13-28 (2010).

Jiang, A., Awasthi, N., Aleksey, N.K., Setyawan, W., Börjesson, A., Bolton, K., Harutyunyan, A.R., Curtarolo, S. Phys. Rev. B, **75**, 205426 (2007).

Kim, S., Jung, J.M., Choi, D.G., Jung, H.T., Yang, S.M., Langmuir, **22**(17), 7109–7112 (2006).

Koetz, J., Kosmella, S., Polyelectrolytes and Nanoparticles , Springer-Velrag Berlin Heidelberg, Germany, 2007.

Kunckels, J., Nuetliche Observationes oder Anmerkungen von Auro und Argento, Potabili, Hamburg, 1676.

Kuno M (2007) Undergraduate inorganic chemistry laboratory, Chem 4M. http://www.nd.edu/~mkuno/Class_downloads/Chem4M_expt2_final.pdf. Accessed on May 26, 2010

Lai, S.L., Guo, J.Y., Petrova, V.V., Ramanath, G., Allen, L.H., Phys. Rev. Lett.., **77**(1), 99-102 (1996).

Leon, Y.R.P., Pichardo, J.L.M., Alcal, O.N., Lopez, R.J.A.,Optical coherence tomography image enhancement by using gold nanoparticles, 22nd Congress of the International Commission for Optics: Light for the Development of the World. Edited by Rodríguez-Vera, Ramón; Díaz-Uribe, Rufino. Proceedings of the SPIE, **8011**, 1-7 (2011).

Lopeandía, A.F., Rodríguez, V.J., Thermochimica Acta, **46**1(1–2), 82–87 (2007).

Luo, Y.C., Do, J.S., Biosens. Bioelectron, **20**, 15-23 (2004).

Mandal, S., Selvakannan, P.R., Phadtare, S., Pasricha, R., Sastry, M., J. Chem. Sci., **114**, 513-520 (2002).

Marbeuf, R. D., Triboulet, R., Journal of Crystal Growth, **117** (14), 1015 (1992).

Markowitz, M.A.,Dunn, D.N., Chow, G.M., Zhang, J., J. Colloid Interface Sci., **210**, 73- 85 (1999).

Martin,J.M., Ohmae, N., Nanolubricants,Wiley,England, 176, 2008.

Mayer, K.M., Lee, S., Liao, H., Rostro, B.C., Fuentes, A., Scully, P. T., Nehl, C.L., Hafner, J.H., ACS Nano, **2**, 687–692 (2002).

Mi, F.L., Shyu, S.S., Kuan, C.Y., Lee, S.T., Lu, K.T., Ajng, S.F., J. Appl. Polym. Sci., **74**, 1868-1879 (1999).

Nakamoto, M., Yamamoto, M., Fukusumi, M., Chem. Commun., 1622-1623 (2002).

Nanda, K.K., Sahu, S.N., Behera, S.N., Phys. Rev. A, **66**, 013208 (2002).

Narayanan, R., El-Sayed, M.A., Phys. Chem. B, **109**(26), 2663-76 (2005).

Nath, N., Chilkoti, A., Anal. Chem., **76**, 5370-5378 (2004).

Nikoobakht, B., El-Sayed, M.A., Chem. Mater., **15** (10), 19571962 (2003).

Park, C., Youn, H., Kim, H., Noh, T., Kook, Y.H. ,Oh, U.T.,Park, H.J., Chulhee, K.J., J. Mater. Chem.,**19**, 2310-2315 (2009).

Pavlov, V., Xiao, Y., Shlyahovsky, B., Willner, I., J. Am. Chem. Soc., **126**, 11768–11769 (2004).

Pedro, B.V., Montewka, K.M., Oles, P.J., Doria, G. ,Franco, R., Clinical Chemistry, **52**, 7 (2006).

Peslherbe, G.H., Ladanyi, B.M., Hynes, J.T., J. Phys. Chem. A, **103**, 2561-2571 (1999).
Potabili, Schutzens, Hamburg, 1676

Pradeep, T., Anshup ,Thin Solid Films, **517**, 6441–6478 (2009).

Rajput, J., Kumar, A.R., Zinjarde, S., Materials Letters, **63** (30), 2672-2675 (2009).

Rinaudo, M., Prog. Polym. Sci., **31**, 603-632 (2006).

Roos, C., Schmidt, M., Ebenhoch, J., Baumann, F., Deubzer, B., Weis, J., **11**, 761-766 (1999).

Roshdi, S., Doaa, A. S., *World Journal of Nano Science and Engineering*, **1**, 51-61 (2011).

Saleh, M., Soliman, H., Haenen, O., Matbouli, E.M., J Fish Dis., **34**(11), 845-852 (2011).

Scaiano, J.C., Billone, P., Gonzalez, C.M., Maretti, L.,Luisa, M.M., McGilvray, K..L., Yuan, N., Pure Appl. Chem., **81**, (4), 635647 (2009).

Songjun, L., Singh, J., He, L., Ipsita, A.B., (Eds.), Biosensor Nanomaterials, John Wiley Sons,Germany, 80, 2011

Sugunan, A., Dutta, J., Novel Synthesis of Gold Nanoparticles in Aqueous Media, in Proceedings of Material Research Society fall conference, MRS, Boston, (1999)

Sun, J., Simon, S.L., Thermochimica Acta, **463** (1–2), 32–40 (2007).

Svergun, D. I., Shtykova, E.V., Dembo, A.T., Bronstein, L.M.,Platonova, O.A., Yakunin, A.N.,Valetsky, P.M., Khokhlov, A.R., J. Chem. Phys. **109**, 111109-11116 (1998)

Tait, H., (Ed.), *Five thousand years of glass* , The British Museum Press, London, 1991.

Teranishi, T., Kiyokawa, I., Miyake, M., Adv. Mater., **10**, 596 (1998).

Turkevich, J., Stevenson, P.C., Hillier, J., Discuss. Faraday. Soc., **11**, 55-75 (1951)

Vohra, M., Grapes, M., Swaminathan, Weihs, T.P., Knio, O.M., J. Appl. Phys., **110**, 123521 (2011).

Wang, R., Yu, Z.W., Acta Physico-Chimica Sinica., **9**,1353-1359 (2007).

Wang, W., Chen, C., Qian, M., Zhao, X.S, Analytical Biochemistry, **373**, 213-219 (2008).

Warad, H.C., Ghosh, S.C.,Thanachayanont, C., Dutta, J., Highly luminescent manganese doped ZnS quantum dots for biological labeling, in Proceedings of International Conference on Smart Materials, Smart/Intelligent Materials and Nanotechnology, SmartMat-'04, Chiang Mai, Thailand, 203–207 (2004)

Willson, J., Beezer, A.E., International Journal of Pharmaceutics, **258**, 77–83 (2003).

Yong, J., Wang, P., Donghong, Y., Liu, J., Qin, L., Yu, N., Xie, G., Li, B., Colloids and Surfaces A: Physicochem. Eng. Aspects, **302**, 366370 (2007).

Zhang, Q., Iwakuma, N., Sharma, P., Moudgil, B.M., Wu, C., McNeill, J.,Jiang, H.,Grobmyer, R., Nanotechnology, **20**, 395102 (2009).

Zhao, W.Y., Lin, L., Hsing, I.M., Langmuir, **26**, 7405–7409 (2010).